ABSTRACT

OJHA, SATYAJEET SOORYAKANT. Fabrication and Characterization of Novel Single and Bicomponent Electrospun Nanofibrous Mats. (Under the direction of Dr. Russell E. Gorga).

Nanofibers were produced using relatively new electrospinning technique. Single layer nanofibers were fabricated using nylon-6. Several parameters such as polymer molecular weight, concentration, surface tension, applied electric voltage, distance between tip to grounded electrode and feed rate were investigated to optimize fiber consistency and diameter. Scanning electron microscopy was employed to study fiber morphology and diameter. Understanding the effects of various parameters mentioned above, electrospinning strategy was further utilized to produce nanofibers with novel core-sheath structure using chitosan, a biopolymer and polyethylene oxide (PEO). Chitosan is very difficult to electrospin, to alleviate this problem PEO was used as sheath to support chitosan core. For this purpose, rheology of polymer solutions was evaluated for successful fabrication of core-sheath nanofibers. Only 3 wt % chitosan was found to produce coaxial structure with 4 wt % PEO, due to their proximity in rheological behavior. Coaxial morphology of nanofibers was verified by transmission electron microscopy having 250 nm and 100 nm as sheath and core diameters respectively. Fourier transform infrared spectroscopy was employed to investigate the effect of de-ionized water treatment of core-sheath mats where in PEO layer was removed off in order to get pure chitosan nanofibers. Coaxial nanofibers with one component were also fabricated using pure PEO as core and PEO doped with Multi-walled carbon nanotubes

as sheath material. Results showed that as carbon nanotubes were subjected to relatively smaller volumes, predominantly on the surface culminated in appreciable increase in conductivity as well as mechanical properties. Coaxial nanofibers produced from electrospinning are of particular interest in tissue engineering and wound healing scaffolds.

FABRICATION AND CHARACTERIZATION OF NOVEL SINGLE AND BICOMPONENT ELECTROSPUN NANOFIBROUS MATS

By

SATYAJEET S. OJHA

A thesis submitted to the Graduate Faculty of

North Carolina State University

in partial fulfillment of the

requirements for the Degree of

Master of Science

TEXTILE ENGINEERING

Raleigh, NC

2007

APPROVED BY

Dr. Russell E. Gorga

(Chair of Advisory Committee)

Dr. Wendy E. Krause

(Committee Member)

Dr. Saad A. Khan

(Minor Representative)

DEDICATION

Dedicated to

Late Shri Arun Lal Ojha

Whose life has always inspired me to achieve

BIOGRAPHY

Satyajeet was born in Jodhpur, India on June 14, 1984 to Sooryakant and Vijaylaxmi Ojha. He received Bachelor of Technology in Fiber and Textile Processing Technology from Mumbai University Institute of Chemical Technology, India. In pursuit of higher studies, he joined North Carolina State University, to start his MS in Textile Engineering in Fall 2005. Upon completion of his MS degree, he plans to join Ph.D. program in Material Science and Engineering at Carnegie Mellon University, Pittsburgh.

ACKNOWLEDGEMENTS

Almighty has been my alter ego in providing me the strength, which enabled me to complete my thesis and research. The completion of this has been made possible through the direct and indirect cooperation of various persons for whom I wish to express my gratitude.

I would like to express my intellectual debt to my advisor, Dr. Russell E. Gorga for all his advice, guidance, encouragement and valuable discussions which made this research possible. It was a knowledgeable experience working with him. I owe my various blocks of learning to Dr. Wendy Krause, who at many times provided me new research ideas, specially related to chitosan. A sincere note of thanks is extended to Dr. Saad Khan for agreeing to be on my committee at last minute notice. I really enjoyed working with Dr. Laura Clarke (Physics) and owe many thanks to her and her group. I am particularly thankful to Dr. Dale Batchelor, Charles Mooney (AIF) and Dr. Michael Dykstra (Vet School) for their continued help with electron microscopy. I am also grateful to Dr. Jan Genzer for being very kind throughout my graduate studies. My colleagues Rebecca Klossner, Jing Liang, Derrick Stevens, Seth McCullen, Torissa Hoffman, Kelly Stano and Dr. Mehdi Afshari deserve my appreciation for extending to me their wholehearted support and assistance in my research.

Heartfelt gratitude to the staff of TECS, Angie Brantley, Judi Elson, Shane Jarvis, Vicki Stocksdale and Birgit Anderson for all their support during my stay here as graduate student.

I am beholden to my grandmother Shakuntala and mother Vijaylaxmi, for their blessings and encouragements. My brothers Piyush and Prashant deserve special acknowledgement for their continuous support through every adventure and challenge. The ability of making sacrifices willingly for me to enable me to work for realizing one of my major ambitions of my life has enabled me to complete this task.

TABLE OF CONTENTS

LIST OF TABLES

Chapter 1

Chapter 4

Chapter 5

Chapter 6

LIST OF FIGURES

Chapter 2

Chapter 4

Chapter 5

Chapter 6

Chapter 1

Background

Electrospinning is a simple and powerful technique to produce fibers at sub-micron level from a number of materials. This simplicity combined with a broad range of materials can be utilized to produce fibers for a variety of applications. Potential applications include nanofibers reinforced composites[1-2], membranes for filteration[3], support for enzymes and catalysts[4] and biomedical applications such as scaffolds for tissue engineering, wound dressings and drug delivery.[5-6]

A large part of American population is approaching old age, as a result of which there is a surge in demand for replacement of organs. Such an increase in demand has encouraged researchers from all realms of science to get together and resolve this issue. So far there is been no or limited success in development of organs generated in-vitro. This issue has initiated an intense research in the field of replacement and development of organs. Table 1 gives information about different procedures performed per patient in USA per year.[1]

Table 1: Outline of the number of procedures per number of patients occurring per year for the United States.

Procedure	**Indication or patients/yr**
Skin	
Burns(*)	2,150,000

Table 1 Contd.

Pressure sores	1,500,000
Venous stasis ulcers	500,000
Diabetic ulcers	600,000
Neuromuscular disorder	200,000
Spinal cord and nerves	40,000
Bone	
Joint replacement	558,200
Bone graft	275,000
Internal fixation	480,000
Facial recontruction	30,000
Cartilage	
Patella resurfacing	216,000
Chondromalacia patellae	103,400
Meniscal repair	250,000
Arthritis (knee)	149,900
Arthritis (hip)	219,300
Fingers and small joints	179,000
Osteochondritis dissecans	14,500
Tendon repair	33,000
Ligament repair	90,000

Table 1 Contd.

Blood vessels	
Heart	754,000
Large and small vessels	606,000
Liver	
Metabolic disorders	5,000
Liver cirrhosis	175,000
Liver cancer	25,000
Pancreas (diabetes)	728,000
Intestine	100,000
Kidney	600,000
Bladder	57,200
Ureter	30,000
Urethra	51,900
Hernia	290,000
Breast	261,000
Bloods transfusion	18,000,000
Dental	10,000,000

Tissue engineering, as Langer describes is "an interdisciplinary field that applies the principles of engineering and life sciences toward the development of biological substitutes that restore, maintain, or improve tissue function."[1] In tissue engineering one

of the most studied areas is tissue engineering scaffolds. It involves replacing diseased or malfunctioning tissues or organs by scaffolds engineered outside the human body and then transplanted into the body at the diseased location. Accomplishment of such a daunting goal necessitates mutual coordination scientists from varied background.

Polymers have been looked upon as the materials of new era. The use of biodegradable and biocompatible polymers for tissue engineering is very highly attractive. Many synthetic polymers have been utilized for fabricating scaffolds such as polyethylene oxide, polyethylene glycol, polyvinyl alcohol to name a few. These scaffolds can have an enormous effect on growth of cells. Fabrication of scaffolds is the first step towards realization of tissue engineering which is followed by cell seeding. Different steps involved in the process are as follows[2]:

I: Fabrication of the bioresorbable scaffold

II: Seeding of cell populations into the polymeric scaffold in a static culture dish

III: Growth of premature tissue in a dynamic environment

IV: Growth of mature tissue in a physiologic environment

V: Surgical transplantation

VI: Tissue-engineered transplant assimilation/remodeling

Given the complex chemistry of human body, the selection of polymer material is very crucial for the success of designed scaffolds. The rate of degradation should be controlled and the products generated by degradation of these scaffolds should also be biocompatible. To issue biocompatibility, many naturally occurring polymers have also been used such as chitosan, hyaluronic acid and alginates as the end products of these

polymers after degradation are absolutely harmless. Following factors are very important while structuring a scaffold[1]:

- Biocompatibility: acceptance within the body without causing biofouling where the body attacks the implant, or the cells do not grow on the material
- Biodegradability: ability to degrade in the body into compatible by-products without causing inflammatory responses
- Mechanical integrity: ability to maintain the original structure and mechanical properties upon exposure to the body's environment, i.e. 37˚C, pH 7.4, saline solution
- High porosity: ability to allow the transfer of nutrients/oxygen and removal of wastes via diffusion
- Bioactivity: ability to transform or conform depending upon the influence from the internal milieu that surrounds the scaffold seeded with cells

Our overall goal through this work is to fabricate scaffolds through electrospinning which potentially could be used in tissue engineering. Nanofibers, produced from electrospinning have favorable surface geometry which facilitates cell adhesion and growth. Through this work we would highlight the utilization of chitosan and multi-walled carbon nanotubes as a novel scaffolding material.

References

1. Kim, J.S., Reneker, D.H., *Polymer Compo.* 1999, 20, 124
2. Bergshoef, M.M., Vansco, G.J., *Adv. Mater.* 1999, 11, 1362
3. Gibson, P., Gibson, H.S., Rivin, D., *Colloids Surf. A,* 2001, 187-188, 469
4. Xie, J., Hsieh, Y-L., *J. Mater Sci*., 2003, 38, 2125
5. Kadler, K.E., Holmes, D.F., Trotter, J.A., Chapman, J.A., *Biochem. J*. 1996, 316, 1
6. Mo, X.M., Xu, C.Y., Kotaki, M., Ramakrishna, S., *Biomaterials*, 2004, 25, 1883
7. R. Lanza, R. Langerand J. Vacanti, *Principles of Tissue Engineering*, Academic Press, Boston, 2000.
8. Hutmacher, *Biomaterials*, **21**, 2529-2543 (2000).

Chapter 2

Literature Review

This chapter provides a comprehensive literature review spanning over many aspects of nanofiber fabrication which forms the backbone of our research. Section 1 gives an overview of "Electrospinning" technique used to fabricate nanocomposite fibers using carbon nanotubes. Section 2 discusses carbon nanotubes, their properties and applications as fillers in nanocomposites. In section 3, an overview of chitosan, a biopolymer having potential applications in tissue engineering when used as scaffolds produced through electrospinning, is discussed. Section 4 focuses on nylon-6 with various spinning parameters and section 5 deals with polyethylene oxide (PEO) and its application in nanofiber fabrication.

2.1. Electrospinning

Electrospinning is a process used to spin fibers having diameter at the sub micron level using an electric field. This is a facile technique to produce nanofibers having potential application in a variety of applications such as drug delivery[1], tissue engineering[2], wound dressings[3] and filtration membranes.[4-5] As a result much research has been done in the last decade on electrospinning which is reflected in number of publications as shown in Figure 1.[6]

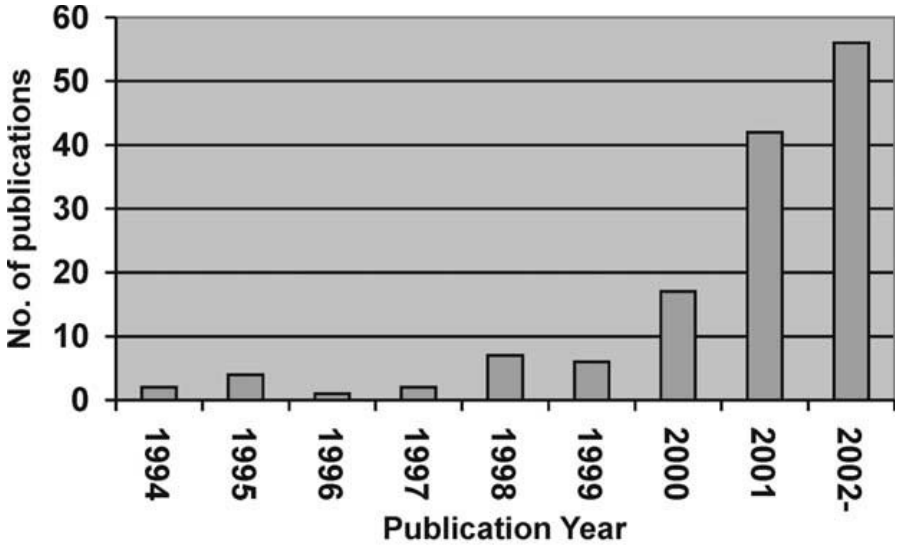

Figure 1. Number of publications in the last decade on electrospinning[6]

The electrospinning process has three primary components, a high voltage supply to charge polymer solution, a grounded electrode where nanofibers are deposited and a syringe with pumps from which the polymer solution is fed through a capillary connected to a syringe filled with the polymer solution. Figure 2 shows a typical electrospinning set-up. In practice, when the polymer solution droplet at the end of capillary is charged to high potential, at a critical value of voltage the droplet overcomes its surface tension and forms a Taylor cone and ejects a tiny jet toward the grounded plate. The axisymmetric instability which causes fibers to break and form undesired beads is known as Rayleigh instability, hence to have continuous nanofibers it needs to be suppressed. Another instability which occurs during electrospinning process is whipping or bending instability, nonaxisymmetric in nature which aids in formation of nanofibers. Rutledge and coworkers has reported a theoretical model explaining these various instabilities.[7-10] Production of nanofibers proceeds through formation of Taylor's cone which is conical in shape.[11] Due to electrostatic attraction nanofibers get collected on grounded electrode. Hence, electrical forces instead of mechanical forces are utilized in spinning of fibers.

Different assemblies of collector electrodes can give oriented or random nanofibers as shown in Figure 3.[41-43] Nanofibers thus obtained in the form of mats have diameter of the order of tens to hundreds of nanometers. Nanofiber mats so formed have a very high porosity (> 60 %) together with very small pore size. Many parameters govern the final morphology of nanofibers such as viscosity and surface tension of the polymer solution, tip to collector distance, voltage and feed rate.[12]

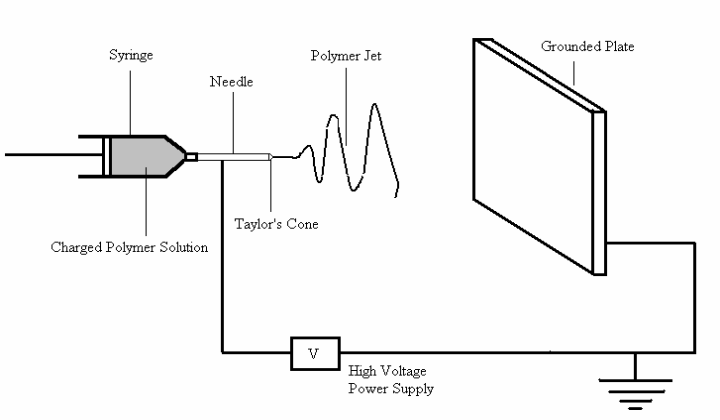

Figure 2. Typical electrospinning set-up

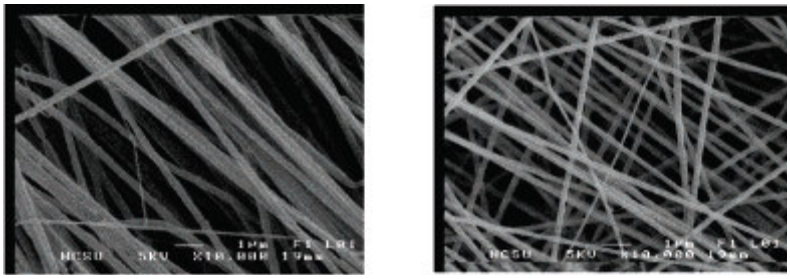

a. Oriented nanofibers b. Random nanofibers

Figure 3. Nanofibers obtained from different collectors (a) parallel bars (b) circular plate[41]

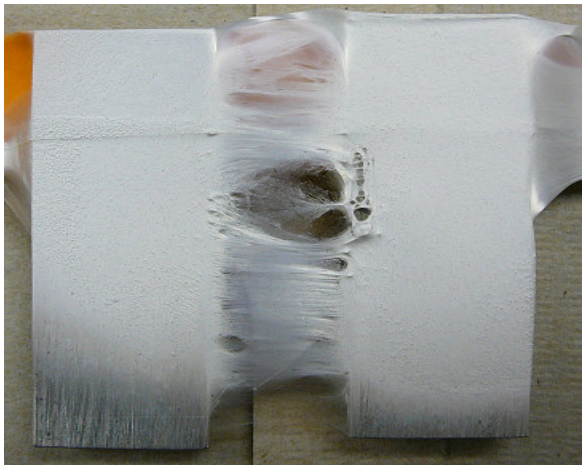

Figure 4. Photograph of aligned nanofibers[44]

In our work, we aim to produce novel nanofibers with high Mw and investigate effects its on mechanical properties of mats. Our interest also lies in fabricating core-sheath nanofibers with different polymer systems. Such a coaxial system would be of immense help in electrospinning nanofibers from polymers which could not be electrospin easily on their own. One of our goals is to attain higher conductivity in core-sheath nanofibers having CNTs in sheath only. Electrospinning apparatus used to produce such nanofibers has been shown in Figure 5 and two perpendicular syringes are used as seen in Figure 6.

Figure 5. Electrospinning set-up for core-sheath nanofibers

Figure 6. Perpendicular syringe system for core-sheath nanofibers

2.2. Carbon Nanotubes

Envisioned as one of the most important discovery of the century by Iijima[13], carbon nanotubes (single- and multi- walled) have generated a great interest in scientific

community. The reason carbon nanotubes have attracted high attention is due to their unprecedented mechanical, electrical and thermal properties. These combined properties make carbon nanotubes an ideal candidate for a variety of applications such as energy storage, energy conversion and semiconductor devices, composites with high strength and conductivity and artificial muscles.[12-17] With so many potential applications of these moieties, there has been a surge in publications and patents issued in the last decade, as shown in Figure 7.[20]

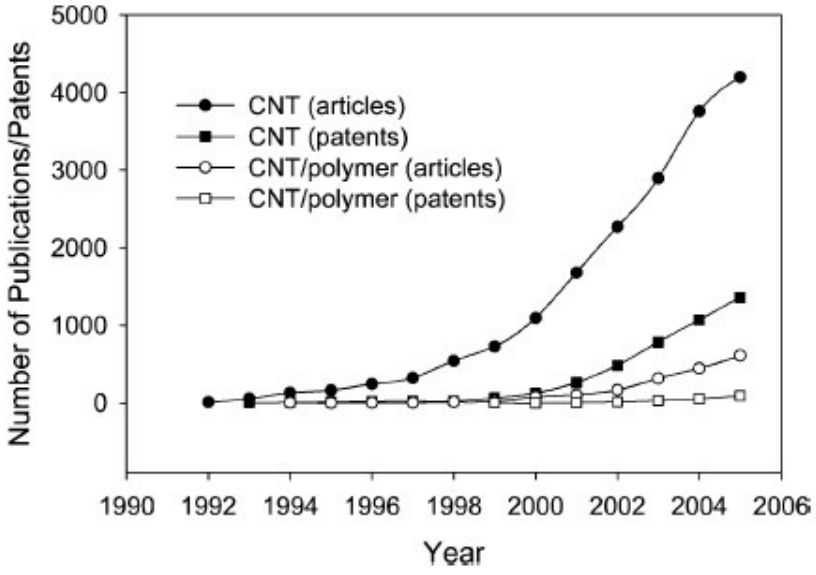

Figure 7. Publications pertaining to CNTs in recent past[20]

2.2.1 Structure and properties of CNTs

Carbon nanotubes are essentially seamlessly rolled graphene sheets having covalently carbon in sp^2 hybridized state. Structurally they can be classified into two categories: Single Walled (SWNT) and Multi-walled (MWNT). SWNTs are single cylindrical structures whereas MWNTs can be assumed as number of SWNTs placed coaxially to

each other with an interlayer separation of 0.34 nm.[21] van der Waals interaction between layers of MWNTs causes a reduction in mechanical strength subject to uiaxial tensile load.[22]

Another classification of carbon nanotubes is made based on surface morphology of these nanotubes. Properties of carbon nanotubes are largely governed by morphological features. The morphology is described by tube chirality or helicity by a circumferential vector C_h (m,n), where m and n are steps along the zig-zag carbon bonds and the chiral angle θ. The chiral angle θ determines the extent of twist in nanotubes. The resulting structure is arm chair if m=n; zig-zag if m=0 or n=0; and chiral for all other combinations of m and n. Fig. 8 shows different morphologies possible in a carbon nanotube.[23] All arm chair and one third of zig-zag nanotubes are metallic in nature having a continuous conduction band, rest two-third zig-zag nanotubes are semiconductor having energy gap in conduction band.[24]

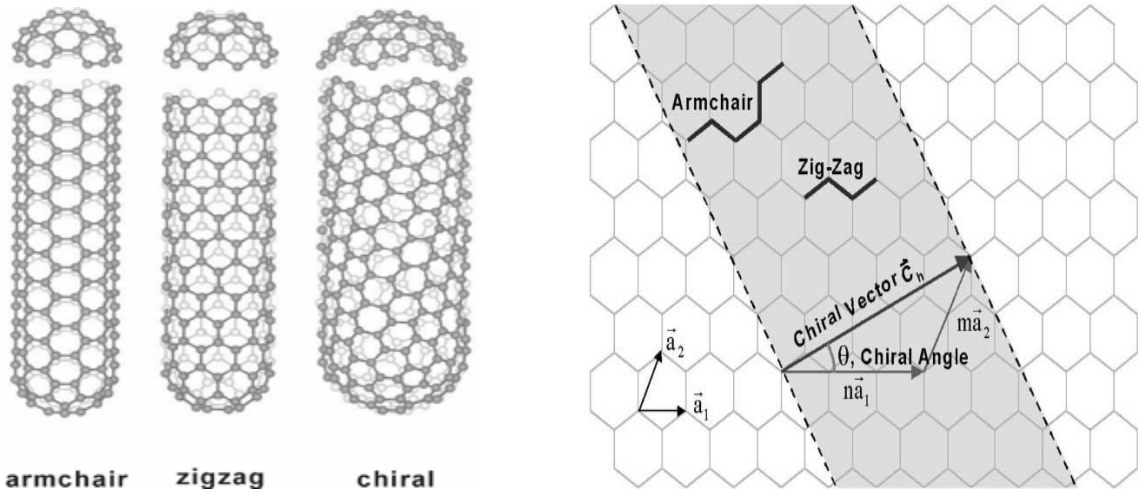

Figure 8. Different morphologies of carbon nanotubes

Carbon nanotubes possess exceptional high flexibility,[25] low mass density,[26] and a very high aspect ratio (>1000). Young's modulus of these nanotubes lies in the range of 1 TPa[27] comparable to diamond whose Young's modulus is 1.2 TPa with a high tensile strength in the range of 150-180 GPa.[28] Treacy et al. used Transmission electron microscopy technique to measure the amplitude to intrinsic thermal vibrations to calculate the moduli (0.41-4.15 TPa) of various MWNTs.[29]

Molecular Dynamics (MD) is an efficient tool to estimate thermal and electrical properties of these nanotubes. Berber et al.[30] found theoretically the thermal conductivity of CNTs (> 6600 W/mK) at room temperature using molecular dynamics whereas Hone and coworkers have experimentally shown a slightly lower thermal conductivity varying between 1750-5800W/mK.[31] Electrical conductivity of these nanotubes lies in the range of 10^6 S/m.[32] All the above properties combined together make carbon nanotubes as exceptional candidate for producing composites with high strength and conductivity properties.

MWNT or SWNT could be produced by three different techniques: Arc discharge, Laser ablation and Chemical Vapor deposition (CVD). Each of these methods has their own advantages and disadvantages. In CVD, nanotubes are grown on a substrate by catalytic decomposition of carbon source and due to a continuous process CVD offers better control over the size and shape of nanotubes as compared to arc discharge or laser ablation. Based on these merits CVD could potentially be employed as a bulk manufacturing technique of nanotubes.[21] In our research experiments, we have used

MWNTs produced from CVD technique having diameter and length 15 ± 5 nm and 5-20 μm respectively with 95 % purity.

To translate above mentioned superior properties of carbon nanotubes into reality, a lot of difficulties need to be overcome. Dispersion of CNTs is an issue of fundamental importance. Since these nanotubes have very high surface to volume ratio, they tend to decrease their surface potential by "bundling together" or agglomeration due to van der Waals attractive forces.[33]Salvetat et al. has found that poor dispersion of CNTs in composites gives rise to poor mechanical properties.[34] Researchers have made several approaches to enhance dispersion such as in-situ polymerization[35-37], covalent functionalization of nanotubes[38] and surfactant aided dispersion using sodium dedecyl benzenesulfonate (NaDDBS), sodium dodecyl sulfate (SDS) to name a few.[39-40] We have utilized surfactant assisted dispersion using ultra sonication with a naturally occurring polysaccharide, *Gum Arabic*. Stable suspension of MWNTs upto 30 days was achieved when gum arabic was used. When gum arabic was not used MWNTs fell out of suspension right after sonication.[41]

A good dispersion together with alignment of nanotubes is a precursor towards stronger nanocomposites with desired properties. Alignment of nanotubes could be achieved either before or during fabrication of nanocomposites. Techniques such as Template,[45-46] Plasma enhanced CVD,[47] Filtration,[48] have been used to align nanotubes before manufacturing . However, external magnetic field or electric field have been used to align nanotubes during fabricating nanotubes.[49-51]

Nanocomposites with appropriate dispersion and alignment of nanotubes would result in efficient transfer of stress from matrix to nanotubes. At low strains, shear stress in the polymer at the interface experiences the same stress as in nanotubes. If the stress increases continuously then at a critical stress the interface will fail. The stress present in the polymer at interface at this point is called as interfacial shear stress.[52] Ajayan et al. first reported nanotubes as fillers in mid 90's.[54] Hwang and coworkers have estimated interfacial shear stress to be 500 MPa for poly (methyl methacrylate) (PMMA)-MWNT system.[53] Toughness increase has been reported by Gorga et al. by inclusion of oriented MWNTs in PMMA[55]

2.3. Chitin and Chitosan

Chitin is a naturally occurring polysaccharide which is produced in highest quantities after cellulose. Chitin is predominantly obtained from animals such as crabs, lobsters and squids to name a few where as, cellulose finds its origin mainly in plants. Chemical structure of chitin ((1→4)-linked 2-acetamido-2-deoxy-β-D-glucopyranose) and cellulose (1→4)-linked- β-D-glucopyranose is very similar as shown in Figure 9. The only difference is presence of –OH group in cellulose on C-2 which is occupied by an acitamido (NHAc) group in chitosan.[56-57] Based on crystalline structure chitin occurs in three forms α, β and γ forms having molecular chains in anti-parallel, parallel and a mixture of parallel and anti-parallel respectively.[58]

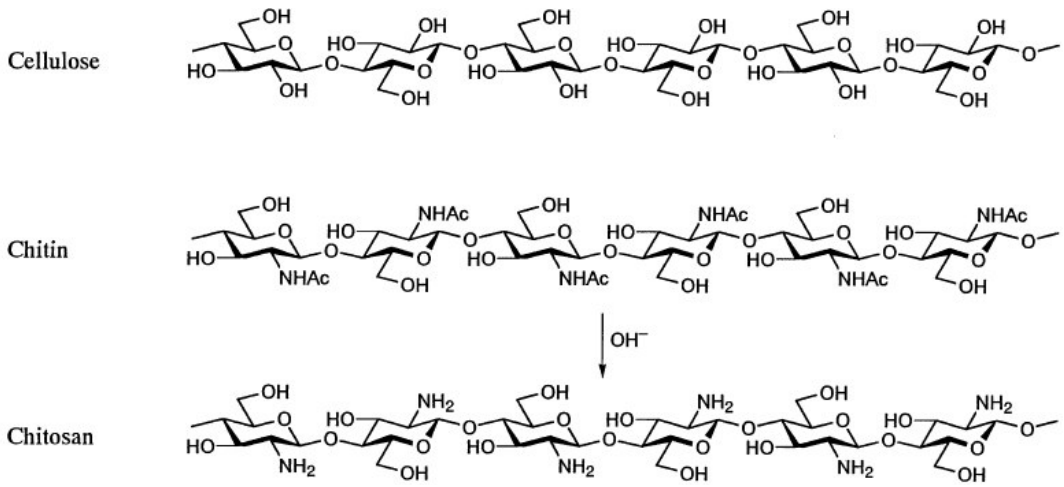

Figure 9. Chemical structure of Cellulose, Chitin and Chitosan[56]

Chitosan (Fig. 9) is a deacetylated form of chitin which is obtained by treatment of chitin with an aqueous alkali (sodium or potassium hydroxide) for few hours at temperatures ranging from 100-160 °C having 70-90 % deacetylation.[59] Presence of reactive amino (-NH_2) group in chitosan is very advantageous as its properties can be tuned by carrying out further chemical modification. Strong inter-chain hydrogen bonding limits solubility of chitin in many solvents and thus rendering chitin difficult to process, however chitosan (deacetylated form of chitin) is soluble in dilute acids such as acetic acid, hydrochloric acid and formic acid.[60] Chitosan has attracted a lot of research in recent past due to its biocompatibility, non-toxicity, anti-microbial nature and accelerated wound healing properties.[61] Chitosan ability to enhance migration of cells such as macrophages, which are crucial in ceasing growth of microorganisms and further immunization, makes it an ideal candidate for wound healing scaffolds.[62] Also chitosan helps attract glycosaminoglycans (GAGS), a growth factor for cell attachment and proliferation, thus acting as an extra cellular matrix (ECM).[63]

Electrospinning has been greatly envisioned as a tool to transform these properties of chitosan into reality. Our main goal is to produce coaxial nanofibers having chitosan, (a biopolymer obtained from crustaceans) as core material in core sheath nanofibers having a prospective application in tissue engineering and wound care.

2.4. Nylon-6

Nylon was first discovered by Wallace Hume Carothers at EI du Pont de Numors. Nylon-6 polymer is produced when a di-acid such as adipic acid is reacts with aminocaproic acid at ~ 260° C as shown in Figure 10.

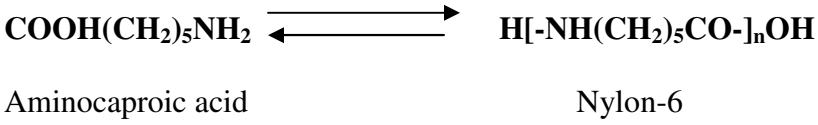

Figure 10. Polymerization reaction of Nylon-6

Nylon is marked by presence of hydrogen bonding between the polymer chains. As a result the chains are packed together giving rise to high melting point, chemical resistance and good mechanical properties. The polymer chains are long straight with no pendant groups or side chains which results in higher degree of order and therefore crystallinity. Nylon, spun with traditional spinning techniques such as melt, dry and wet spinning has molecular weight in the range of 12,000-20,000 gm/mol. In melt spinning, polymer in the form of chips is heated above its melting point and then the melt is forced

through small apertures called as “dies”. Fine fibers are obtained by subsequent cooling. At higher molecular weights (> 20,000), processing of polymer into fibers is challenging due to difficulty in melting the polymer compounded by high viscosity arising from entanglement of polymer chains.[64-65]

In dry spinning polymer is dissolved in a certain solvent or a mixture of solvent and during spinning due to low boiling point, solvent evaporates leaving behind polymer in the form of fibers. This process is costlier than melt spinning process as extra equipments are required for making polymer-solvent mixture and solvent recovery. Higher molecular weight polymer can be spun with this method.[65] Tensile strength of 1 GPa with a draw ratio of 10 for nylon-6 has been reported in literature.[66] Wet spinning also works on same principle but instead of evaporation of solvent as in dry spinning, here solvent is leached in a coagulation bath. With respect to dry spinning, wet spinning is more complicated as proper choice of coagulant is needed which can precipitate the solvent in coagulating bath.

New technique such as gel spinning has also been reported in literature. In gel spinning the polymer in the form of gel is spun having low entanglement density which is further cooled down to solidify. Fibers can be drawn to high draw ratios using gel spinning in order to achieve higher strength. Cho and coworkers have utilized gel spinning to produce high strength nylon-6 fibers having modulus of 6.2 GPa.[67]

In our work, we have spun nylon nanofibers using electrospinning with different molecular weights (30,000, 50,000 & 63,000 gm/mol). Chapter 2 elaborates our work in more detail.

2.5. Polyethylene oxide (PEO)

Electrospinning of Polyethylene oxide (PEO) has been investigated in great detail by many researchers. It is soluble in a variety of solvents such as water, dimethyl formamide (DMF), ethanol and chloroform.[68] Biocompatibility and non-toxicity are two key properties which render PEO as a suitable biomaterial for application in areas such as tissue engineering and wound scaffolds. PEO has served as an ideal candidate to gain a fundamental understanding of effect of various parameters during electrospinning such as applied voltage, solution flow rate, distance between tip and grounded electrode and solution properties such as viscosity, conductivity and surface tension. Dieztel et al. have shown that solution properties play an important role on structure and morphology of resulting nanofibers.[69-70] Versatility of PEO in electrospinning has been crucial in processing of polymers which cannot be electrospun on its own such as chitosan, proteins, alginate and hyaluronan.[71-76] McDiarmid et al have electrospun PEO with polyaniline doped with camphorsulphonic acid to produce conducting nanofibers.[77]

Using PEO as a template, through our work we have been able to produce core-sheath nanofibers having chitosan as core and PEO as sheath. Here PEO has acted as a template to get chitosan nanofibers. Detailed investigation has been elaborated in chapter 3.

2.6 References:

1. Kenawy, E.R., Bowlin, G.L., Mansfield, K., Layman, J., Simpson, D.G., Sanders, E.H., Wnek, G.E., *J. Controlled Release* 2002, 81, 57
2. Chen, J., Karageorgiou, V., Altman, G.H., Kaplan, D.L., *Biomaterials* 2004, 25 1039
3. Khil, M.S., Cha, D.I., Kim H.Y., Kim, I.S., Bhattrai, N., J. *Biomed. Mater. Res. Part B: Appl. Biomater.* 2003, 67B, 675
4. Tsai, P.P., Schreuder-Gibson, H., Gibson, P., *J. Electrostat.* 2002, 54, 333
5. Shao, C., Kim, H.Y., Gong, J., Ding, B., Lee, D.R., Park, S.J., *Mater. Lett*. 2003, 57, 1579
6. Huang, Z.M., Zhang, Y.Z., Kotaki, M., *Comp. Sci. and Tech.* 2003, 63 (15): 2223
7. Shin, Y.M., Hohman, M.M., Brenner, M.P., Rutledge, G.C., *Polymer* 2001, 4, 9955
8. Hohman, M.M., Shin, M., Rutledge, G.C., Brenner, M.P., *Phys. Fluids,* 2001, 13:2201
9. Hohman, M.M, Shin, M., Rutledge, G.C., Brenner, M.P., *Phys. Fluids* 2001,13:2221
10. Shin, Y.M., Hohman, M.M., Brenner, M.P., Rutledge, G.C., *Appl. Phys. Lett.* 2001, 78:1149–
11. Taylor G.I., *Proc. R. Soc. Lond. Ser. A* 1969, 313, 453
12. Fong, H., Chun, I., Renker, D.H. *Polymer*, 1999, 40, 4585
13. Iijima, S., *Nature*, 1991, 354, 56
14. Baughman, R.H. *Science*, 2003, 300, issue 5617, 268

15. An, K.H., Kim, W.S., Park, Y.S., Moon, J.M., Bae, D.J., Lim, S.C., Lee, Y.S., Lee, Y.H., *Adv. Funct. Mater.* 2001, 11, 387

16. Niu, C., Sichel, E.K., Hoch, R., Moy, D., Tennent, H., *Appl. Phys. Lett.* 1997, 70, 1480

17. Baughman, R.H. Cui, C., Zakhidov, A.A., Zafar, I., Barisci, J.N., Spinks, G.M., Wallace, G.G., Mazzoldi, A., Rossi, D.D., Rinzler, A.G., Jaschinski, O., Roth, S., Kertesz, M., *Science,* 1999, 284, 1340

18. Biercuk, M.J., Llaguno, M.C., Radosavljevic, M., Hyun, J.K., Johnson, A.T., *Appl. Phys. Lett.* 2002, *80*, 2767

19. Lau, K.T. and Hui, D. *Composites Part* B 2002, 33, 263.

20. Moniruzzaman, M., and Winey K.I.**,** *Macromolecules* 2006**,** *39,* 5194

21. Awasthi, K., Srivastava, A., Srivastava, O. N., *J. Nanosci. Nanotechnol.* 2005, *5*, 1616

22. Lau K.-T., Gu, C., Hui, D., *Composites: Part B* 37, 2006, 425

23. Thostenson, E.T.; Zhifeng, R.; Chou, T.-W., *Compos. Sci. Technol.* 2001, *61*, 1899

24. Harris, P.J.F. Carbon Nanotubes and Related Structures, 1999, Cambridge University Press, Cambridge, UK.

25. Cooper, C. A.; Young, R. J.; Halsall, M. *Composites, Part A* 2001, 32A, 401

26. Gao, G.; Cagin, T.; Goddard, W. A., III. *Nanotechnology* 1998, 9, 184

27. Treacy, M.M.J., Ebbesen, T.W. and Gibson, J.M. *Nature,* 1996, 381, 6584, 678

28. De Heer Walt, A. *MRS Bull.* 2004, *29*, 281-285.

29. Treacy, M.M.J., Ebbesen, T.W., Gibson, J.M., *Nature* 1996, 381, 678.

30. Berber, S.; Kwon, Y.-K.; Tomanek, D. *Phys. Re*v. *Lett.* 2000, 84, 4613

31. Hone, J., Whitney, M., Piskoti, C. and Zettl, A. *Physical Review B*, 1999, 59(4): R2514

32. *Phys. Rev. Lett.*, **82** (1999)

33. Qian, D., Dickey, E.C., Andrews, R., Rantell, T., *Appl. Phys. Lett*. 2000, 76, 2868.

34. Salvetat, J.P., Briggs, A.D., Bonard, J.M., Bacsa, R.R., Kulik, A.J., Stockli, T., Burnham, N.A., Forro´, L., *Phys. Rev. Lett.* 1999, 82 944

35. Tang, B.Z., Xu, H.Y., *Macromolecules* 1999, 32 2569

36. Star, A., Stoddart, J.F., Steuerman, D., Diehl, M., Boukai, A., Wong, E.W., Yang, X., Chung, S.W., Choi, H., Heath, J.R., *Angew. Chem. Int. Ed*. 2001, 40 1721

37. Jang, J., Bae, J., Yoon, S.H., *J. Mater. Chem.* 2003, 13, 676

38. Mitchell, C.A., Bahr, J.L., Arepalli, S., Tour, J.M., Krishnamoorti, R. *Macromolecules* 2002, *35*, 8825

39. Islam, M.F.; Rojas, E.; Bergey, D.M.; Johnson, A.T.; Yodh, A.G., *Nano Lett.* 2002, *3*, 269

40. Vigolo, B., Penicaud, A., Coulon, C., Sauder, C., Pailler, R., Journet, C., Bernier, P., Poulin, P., *Science* 2000, 290, 1331

41. McCullen, S.D., Stevens, D.R., Roberts, W.A., Ojha, S.S., Clarke, L.I., Gorga, R.E., *Macromolecules*, 2007, 40 (4), 997

42. Boland, E.D., Wnek, G.E., Simpson, D.G., Palowski, K.J., Bowlin, G.L., J. *Macromol. Sci. Pur. Appl. Chem*., 2001, A38 (12), 1231

43. Theron, A., Zussman, E., Yarin, A.L., *Nanotechnology*, 2001, 12, 384

44. Ojha, S.S., Gorga, R.E., *unpublished work*

45. Li, J., Papadopoulos, C., Xu, J.M., Moskovits, M., *Appl. Phys. Lett*. 1999, 75, 367

.

46. Wang, X.B., Liu, Y.Q., Hu, P.A., Yu, G., Xiao, K., Zhu, D.B., *Adv. Mater*., 2002, 14, 1557

47. Ren, Z.F., Huang, Z.P., Xu, J.W., Wang, J.H., Bush, P., Siegal, M.P., Provencio, P.N., *Science,* 1998, 282, 1105

48. W.A. de Heer,W.S. Bacsa, A. Chatelain, T. Gerfin, R. Humphrey-Baker, L. Forro, D. Ugarte, *Science*1995, 268, 845

49. Choi, E.S., Brooks, J.S., Eaton, D.L., Al-Haik, M.S., Hussaini, M.Y., Garmestani, H., Li, D., Dahmen, K., *J. Appl. Phys.* 2003, 94, 6034

50. Dror, Y., Salalha, W., Khalfin, R.L., Cohen, Y., Yarin, A.L., Zussman, E., *Langmuir* 19 (2003) 7012

51. Reneker, D.H. Chun, I., *Nanotechnology* 1996, 7, 216

52. Kelly, A., Macmillan, N. H., *Strong Solids*, 3rd ed., Oxford University Press, 1986, Oxford, UK

53. Hwang, G. L., Shieh, Y.-T., Hwang, K. C., *Adv. Funct. Mater.* 2004, *14*, 487

54. Ajayan, P. M.; Stephan, O.; Colliex, C.; Trauth, D. *Science* 1994, *265*, 1212

55. Gorga, R.E., Cohen, R.E., *Journal Of Polymer Science Part B-Polymer Physics*, 2004, 42, 2690

56. Kurita K., *Prog. Polym. Sci*., 2001, 26, , 1921

57. Kurita K., *Marine Biotechnology*, 2006, 8 (3), 203

58. Rudall K.M., Kenchington W., *Biol. Rev*. 1973, 49, 597

59. Hudson, S.M., Jenkins, D.W., “Chitin and Chitosan." Encyclopedia of Polymer Science and Technology, 3rd Ed., 2001, Herman F. Mark. Hoboken, NJ: Wiley Interscience

60. Senel, S., McClure, S. J., *Advanced Drug Delivery Reviews* 2004, 56.10 1467

61. Lim, S.-H., Hudson, S. M. *Journal of Macromolecular Science-Polymer Reviews,* 2003, C 43(2), 223

62. Ueno, H., T. Mori, and T. Fujinaga. *Advanced Drug Delivery Reviews* 52.2 2001, 105-115.

63. Di Martino, Alberto, Sittinger M., and Makarand V. Risbud. *Biomaterials* 2005, 26 5983

64. Moncrieff, R.W., Man Made Fibers, 1970, 5th ed., John Wiley & Sons Inc. New York

65. Hufnagel, D., Hyaluronic acid-based nanofibers via electrospinning, *MS Thesis*, 2006, North Carolina State University

66. Gogolewski, S., Pennings, A. J., *Polyme*r, 1985, 26, 1394

67. Cho J. W., Lee G. W., Chun B. C., *J. Appl. Polym. Sci.,* 1996, 62, 771

68. Brandrup, J., Immergut, E.H., Polymer handbook, 1975, 2nd ed., John Wiley & Sons Inc. New York

69. Deitzel, J.M., Kleinmeyer, J., Harris, D., Beck Tan, N.C., *Polymer* 2001, 42, 261

70. Deitzel, J.M., Kleinmeyer, J., Harris, D., Beck Tan, N.C., *Polymer* 2001, 42, 8163

71. Bhattarai, N., Edmondson, D., Omid V., Matsen, F.A., Zhang, M., *Biomaterials*, 2005, 26, 6176

72. Duan, B., Dong C., Yuan, X., Yao, K., *J. Biomater. Sci. Polymer Ed*., 2004, 15 (6), 797

73. Bhattarai, N., Li, Z., Edmondson, D., Zhang, M., *Adv. Mater.* 2006, 18, 1463

74. Ji, Y., Ghosh, K., Shu, X.Z., Li, B., Sokolov, J.C., Prestwich, G.D., Clark, R.A.F., Rafailovich, M.H., *Biomaterials*, 2006, 27, 3782

75. Xie, J., Hsieh, Y.L., *J Mater Sci* 2003, 38, 2125

76. Jian, H.J., Fridrikh, S.V., Rutledge, G.C., Kaplan, D.L., *Biomacromolecules,* 2002, 3, 1233

77. Norris, D., Shaker, M.M., Ko F.K., MacDiarmid, A.G., *Synth Met* 2000, 114, 109

Chapter 3

Research Objectives

3.1 Research Objectives

Electrospinning has evolved as a facile technique to produce materials finding applications in a number of fields. A better understanding of the procedure in terms of solution and process parameters is vital for further development of this technique which would help to transform it from laboratory to commercial scale. How do we get fine and uniform nanofibers from polymer solutions? Could this technique be used to produce nanofibers with coaxial morphology? Once nanofibrous mats are produced, how their properties can be utilized rendering them useful for applications such as tissue engineering? What role is played by carbon nanotubes in altering the conducting properties of nanofibrous mats? These would be few questions we would attempt to answer through our work.

The number of Americans on the waiting list has doubled from 1995 to 2005 due to the scarcity of available resources as reported by U.S Scientific Registry of Transplant Recipients. Such inadequacy has resulted into a substantial research thrust in areas like tissue engineering. It has now become important to continuously look for functional materials as scaffold in tissue engineering. For this research we will attempt to gain an insight into the fundamentals of electrospinning and thereby develop an understanding of the process in order to produce novel scaffolds with desired properties. For this purpose, chitosan, a naturally occurring polysaccharide has been investigated. Specifically, the research objectives are as follows:

1. Fabricate nanofibers via electrospinning as a measure to understand effects of various parameters involved in the process. This will be accomplished by:
    a. Analyzing of effect of molecular weight, concentration, viscosity and surface tension.
    b. Determining the consequences of variation in applied electric field, voltage and feed rate of polymer solution.
    c. Analyzing the electrospun nanocomposites via scanning electron microscopy to confirm proper fiber formation.
    d. Determining any improvements in mechanical properties via tensile testing.
2. Fabricate novel nanofibers with core-sheath geometry for potential application in tissue engineering. This will be accomplished by:
    a. Engineering a model to produce core-sheath nanofibers.
    b. Using Chitosan, a biopolymer with Poly ethylene oxide (PEO).
    c. Analyzing the rheological properties of two polymer solution (Chitosan and PEO) using rheometer.
    d. Analyzing the electrospun nanocomposites via scanning and transmission electron microscopy to confirm proper fiber formation.
    e. Determining change in conductance as a result of wetting the coaxial nanofibers.
    f. Ascertaining any change in mechanical properties as a result of insertion of chitosan as core in nanofibers.
3. Fabircating core-sheath nanofibers using a single polymer system with core as

pure polymer and sheath as polymer doped with multi-walled carbon nanotubes for enhanced electrical conductivity. This will be accomplished by:

a. Determining the rheological properties of the polymer solutions and the effect of multi-walled carbon nanotube addition
b. Analyzing the electrospun nanocomposites via scanning and transmission electron microscopy to confirm proper fiber formation and multi-walled carbon nanotube integration into the as-spun fiber.
c. Determining any improvements in mechanical properties and electrical conductivity via tensile testing and sensitive conductivity measurements, respectively.

Chapter 4

Morphology and mechanical properties of electrospun nylon-6 nanofibers as a function of molecular weight and processing parameters

Satyajeet S. Ojha, Mehdi Afshari, Richard Kotek, & Russell E. Gorga[1]

Fiber and Polymer Science, College of Textiles, North Carolina State University, Raleigh, NC 27695-8301-USA

4.1. Abstract

In the present study, the morphology and mechanical properties of nylon-6 nanofibers were investigated as a function of molecular weight (30,000, 50,000 and 63000 gm/mol) and the electrospinning process conditions such as the effect of solution concentration, applied electric field strength and distance between tip of needle and collector were also studied. Non-woven mats were successfully electrospun from 15 wt % solutions of each molecular weight polymer. Scanning electron micrographs (SEM) of nylon-6 nanofibers showed the diameter of the electrospun fiber increased with increasing molecular weight and solution concentration. An increase in molecular weight increases the density of chain entanglements at the same concentration hence, the minimum concentration to produce nanofibers was lower for the highest molecular weight nylon-6. The morphology of electrospun fibers also depended on tip-to-collector distance and applied voltage concentration of polymer solution as observed from the SEM images. Mechanical properties of electrospun nonwoven mats showed an increase of 50 % in Young's modulus with increasing Mw of nylon-6.

[1] Corresponding Author: Tel:+1-919-515-6553
E-mail: regorga@ncsu.edu

Keywords: electrospinning, molecular weight, nanofibers, morphology, mechanical properties

4.2. Introduction

Conventional fiber spinning techniques such as wet spinning, dry spinning, melt spinning, and gel spinning can produce polymer fiber with diameters down to the micrometer range. If the fiber diameter is reduced from micrometers to nanometers, very large surface area to volume ratios can be obtained. These unique qualities make polymer nanofibers an optimal candidate for many important applications [1]. Polymer fibers can be generated from an electrostatically driven jet of polymer solution or polymer melt. This process, known as electrospinning, has received a great deal of attention in the last decade because of its ability to consistently generate polymer fibers that range from 50 to 500 nm in diameter [2-5]. Because of the small pore size and high surface area inherent in electrospun textiles, these fabrics show promise for exploitation in soldier protective clothing (to help maximize the survivability, sustainability, and combat effectiveness of the individual soldier system against extreme weather conditions, ballistics, nuclear, biological and chemical warfare). Filtrations, membrane, reinforcing fibers in composite materials, optical and electronic applications (piezoelectric, optical sensor) are other fields where they could be of potential application. Drug delivery with polymer nanofibers is based on the principle that dissolution rate of a particulate drug increases with increasing surface area of both the drug and the corresponding carrier. Many biomedical devices of practical uses (cosmetics: skin healing and skin cleansing, wound dressing, drug delivery and pharmaceuticals) can be fabricated with nanofibers. They

could also be used as supports for enzymes or catalysts and scaffold for tissue engineering and templates for the formation of hollow fibers with inner diameters in the nanometer range [6-14].

A high electrical potential, typically 10-20 kilovolts, is applied to a polymer solution in syringe. Due to high electric field jet whips around, and stops at the grounded collection region [1]. The base is the region where the jet emerges from the liquid polymer. The geometry of the jet, near the base, is a tapered Taylor cone in which the axial velocity of the liquid increases as the polymer is accelerated along the axis of the jet. If the electric field is strong enough, a jet of liquid can be ejected from a pendant drop that was essentially circular before the field is applied. The jet is the region beyond the base where the electrical forces continue to accelerate the polymer liquid and then stretch the jet. In this region, the diameter of the jet decreases and the length increases in a way that keeps constant the amount of mass per unit time passing any point on the axis [1]. Analysis of the flow field in an electrically driven jet showed that the region about the symmetry axis of the jet is free of rotational components and is thus an area of pure extensional flow [15]. The collection region is where the jet is stopped. The polymer fibers that remain after the solvent evaporates may be collected on a metal screen. The initiation and formation of the jet is a complex and interesting process with many variations [7]. In electrospinning process the morphology of the fibers depends on the various parameters such as solution concentration, applied electric field strength and tip-to-collector distance [16-18]. Although research has provided a fundamental understanding of the process, the

fiber morphology as a function of solution properties (concentration, polymer molecular weight) and processing conditions is not well quantified.

Many parameters can influence the transformation of polymer solutions into nanofibers through electrospinning. These parameters include: a)The solution properties such as viscosity, elasticity, conductivity, and surface tension, b)governing variables such as hydrostatic pressure in the capillary tube, electric potential at the capillary tip, and the gap (distance between the tip and the collecting screen), and c) ambient parameters such as solution temperature, humidity, and air velocity in the electrospinning chamber [9].

Sometimes electrospun fibers exhibit bead-on-string structures, which have been generally considered to be undesirable by-product or defects. Theoretical analysis in the literature predicted three types of instabilities for an electrically driven jet: axisymmetric Rayleigh instability, electric field-induced axisymmetric instability, and whipping instability. Bead formation results from axisymmetric instabilities and flow of the electrospun jet. Specifically, applied voltage, solution surface tension, and conductivity can influence the formation of beaded fibers [19]. For poly hydroxybutyrate-co-valerate (PHBV) electrospun fibers Zuo and coworkers [19] showed that higher applied voltage favor formation of smooth fibers and beads are likely to be formed at high feed rate. High surface tension promotes the formation of PHBV electrospun fibers with beads, whereas increased conductivity favors uniform smooth fibers.

Among the many eletrospun polymers reported in the scientific literature are poly(p-phenylene terephthalamide) [37], tri-block polymers [39], Nylon [22-29], polyethylene oxide and DNA from solution [38]; polyethylene and polypropylene from the melt [40]. Nylon has been widely used as an important engineering plastic because of its good mechanical properties. Nylon fibers have been produced by traditional methods such as melt, wet and dry spinning. These fibers are available in staple, tow, monofilament and multifilament form [20]. Fiber diameters produced by these methods range from 10 to 500 micrometer [21].

Ryu and coworkers [22] examined morphology, pore size, surface area and gas transport properties of nylon 6 nonwoven electrospun mats. The crystallinity of nanocomposites of nylon-6 and montmorillonite clay was studied by Fong et.al [23]. The ultra large draw ratio and rapid solvent removal of electrospinning favors the formation of γ-phase nylon crystallites in pure nylon-6 and montmorillonite-nylon-6 fibers [23]. Bregshoef and Vancso [8] prepared nanocomposites with ultrathin, electrospun nylon-4,6 fibers and compared mechanical properties of nylon 4,6/epoxy composite films and epoxy films.

Larrondo and coworkers [24] in an effort to understand the mechanism of jet formation from polymer melts with the aid of an electric field used molten polymers of nylon-12 and polyethylene. The drop formation was measured as a function of field intensity and frequency.

Gibson and coworkers [25] used Nylon-66, Polybenzimidazole and Polytetrafluoroethylene membranes from electrospun fibers as protective layers. They measured properties of electrospun membranes including structural effects upon moisture transport, air convection, aerosol filtration, porosity, tensile strength.

Using Raman spectroscopy Stephen and coworkers [26] showed that in the case of nylon-6 polymer crystalline structure was altered from α to γ form when electrospun. This however is not a permanent conformational change and can be converted back to α form by solvent casting a film from the electrospun membrane. The ability of the electrospinning process to produce the γ form implies that the fibers are under high stress when they are being formed. For nylon-12 that only has one preferred conformation, the chain conformation is conserved after processing.

Supaphol and coworkers [27-29] studied the effects of electrode polarity and processing parameters on morphological appearance and size of the as-spun nylon-6 fibers. An increase in the temperature of the spinning solutions decreased the size of the as-spun fibers. Addition and increasing content of NaCl caused the conductivity of the spinning solutions to increase which in turn, caused the sizes of the as-spun fibers to increase. Fibers obtained from nylon-6 of higher molecular weights appeared to be larger in diameter. The maximum molecular weight they used was 32000 g/mol with varying concentration (10-46 % w/v). An increase in the temperature of the solution during electrospinning resulted in a decrease in the fiber diameters. Increasing solution viscosity resulted in a reduced number of beads and increased fiber diameters. Diameters of fibers

obtained under the negative electrode polarity were larger than those obtained under the positive electrode polarity.

Dersch [30] showed that intrinsic structure of nylon-6 and polylactic acid (PLA) fibers do not differ to an appreciable extent from those found for much thicker fibers obtained by melt extrusion. The annealing of polyamide fibers at elevated temperatures resulted in a transformation from the disordered γ from to the more highly ordered α form. The orientation of the crystals along the fiber axis was strongly inhomogenous: it was an average, very weak. A brief note is made on the research done on nylon-6 with major focus area is shown in Table 1.

Table 1. A brief review of studies conducted on different types of nylon.

Author	Polymer	Solvent	Mw (g/mol)	Focus	Reference
Supaphol	N6	Formic acid, m-chresol, sulphuric acid	17000, 20,000, and 32000	Effects of solvent, polarity of electrode, concentration, and addition of salt (NaCl)	27-29
Gibson	N66	Formic acid	Not reported	Properties of electrospun membranes (moisture transport, air convection, aerosol filtration, tensile strength)	25
Larrondo	N12	-	35000	Modeling of drop formation in terms of a theory Troza	24
Stephen	N6, N12	HFIP	N6: 43,300 N12: 32000	Investigation about chain conformation during electrospinning by Raman spectroscopy	26
Dersch	N6	Formic acid	Not reported	Comparison structure of electrospun and melt spun fibers by x-ray	30
Fong	N6	HFIP, HFIP/dimethyl formamide	20,000	Effects of solvent	23
Bregshoef	N46	Formic acid	Not reported	Transparent composite	8

In the present study we investigated effect of voltage, distance between collector and tip of syringe and solution concentration of 3 different molecular weight of PA-6 (30,000, 50,000 and 63000 g/mol) in formic acid on diameter of electrospun fibers of PA-6. In the literature published the highest molecular weight that has been utilized to produce nanofibers is 32000 g/mol [27]. We have made the first attempt to produce high molecular weight PA-6 up to 63000 g/mol in order to comprehend the effect of molecular weight on morphology of nanofibers and mechanical properties of electrospun nonwoven mats.

4.3. Experimental

4.3.1. Materials

Three molecular weights of nylon-6 were investigated (high (63000 g/mol), medium (50000 g/mol) and low (30000g/mol) molecular weight (ULTRAMID BS700, BS3301 and B4001) from BASF). The viscosity averaged molecular weight was calculated from the Mark-Houwink equation (1).

$$[\eta] = KM_w^{\,a} \qquad (1)$$

The constants *K* and *a* values used for the nylon-6/formic acid system at 25 °C were 22.6 × 10^{-5} dL/g and 0.82, respectively [36]. The viscometric measurements were conducted at 25°C by using an Ubbelohde viscometer. The limiting viscosity number was determined from the following equation (2):

$$[\eta] = \frac{2}{C}(\eta_{rel}^{1/2} - 1) \qquad (2)$$

Here C is polymer concentration, $[\eta]$ is intrinsic viscosity and η_{rel} is relative viscosity.

Two polymer solution concentrations 10 wt % and 15 wt % prepared by dissolving nylon-6 in Formic acid (Merck). Samples of different molecular weight and concentrations with varying processing parameters were used. Table 2 shows sample code and processing parameters of samples. The samples code can be identified as:

1. Molecular weight LMW, MMW, and HMW refers to low, medium and high molecular weight nylon-6, respectively.
2. Concentration C_1 and C_2 refers to 10 and 15 wt%, respectively.
3. Voltage V_1, V_2, and V_3 refers to 10, 15, and 20 kV, respectively.
4. Distance from tip to collector D_1, D_2, and D_3 refers to 10, 15, and 20 cm, respectively.
5. Feed rate F_1, F_2, and F_3 refers to 15, 50, and 100 µl/min, respectively.

For example $LMWC_1V_2F_1D_2$ refers to nanofibers produced from low molecular weight nylon-6 having 10 wt% concentration, at 15 kV voltage, 15 µl/min feed rate, and 15 cm distance.

Table 2: Sample Codes and processing parameters used in the experimental study

Sample Code	**Mol. Wt. (g/mol)**	**Concentration (wt %)**	**Voltage KV**	**Feed Rate µl/min**	**Distance cm**
$LMWC_1V_2F_1D_2$	30000	10	15	15	15
$MMWC_1V_2F_1D_2$	50000	10	15	15	15
$HMWC_1V_2F_1D_2$	63000	10	15	15	15
$LMWC_2V_2F_1D_2$	30000	15	15	15	15

Table 2 Contd.

$MMWC_2V_2F_1D_2$	50000	15	15	15	15
$HMWC_2V_2F_1D_2$	63000	15	15	15	15
$LMWC_2V_1F_1D_2$	30000	15	10	15	15
$LMWC_2V_3F_1D_2$	30000	15	20	15	15
$MMWC_2V_1F_1D_2$	50000	15	10	15	15
$MMWC_2V_3F_1D_2$	50000	15	20	15	15
$HMWC_2V_1F_1D_2$	63000	15	10	15	15
$HMWC_2V_3F_1D_2$	63000	15	20	15	15
$LMWC_2V_2F_1D_1$	30000	15	15	15	10
$LMWC_2V_2F_1D_2$	30000	15	15	15	15
$LMWC_2V_2F_1D_3$	30000	15	15	15	20
$HMWC_2V_2F_1D_3$	63000	15	15	15	20
$MMWC_2V_2F_2D_2$	50000	15	15	50	15
$MMWC_2V_2F_3D_2$	50000	15	15	100	15
$HMWC_2V_2F_2D_2$	63000	15	15	50	15
$HMWC_2V_2F_3D_2$	63000	15	15	100	15
$HMWC_1V_2F_2D_2$	63000	10	15	50	15

4.3.2. Electrospinning

For electrospinning of nylon-6, a variable high voltage power supply (Glassman high voltage model # FC60R2 with positive polarity) was used as a power supply to apply voltages of +10, +15 and +20 kV to the horizontal oriented syringe tip. The polymer

solution was place in a 10 ml syringe to which a capillary tip of 0.4 mm inner diameter was attached. The positive electrode of the high voltage power supply is connected to the capillary tip. The grounded electrode was connected to a metallic collector wrapped with aluminum foil as shown in Fig. 1.

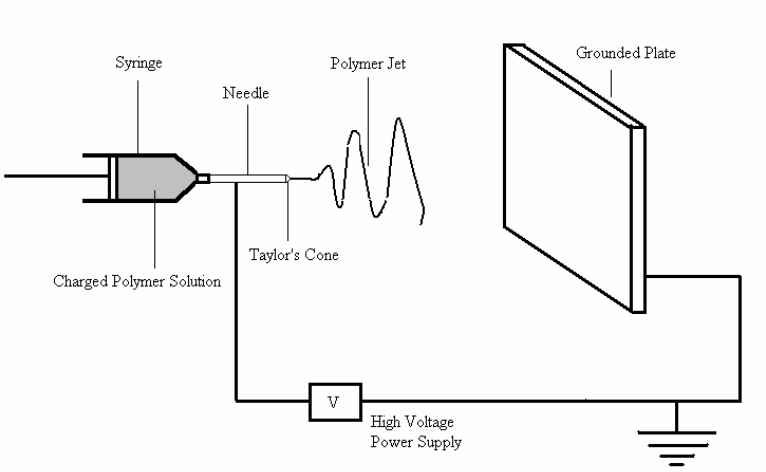

Figure 1: Typical electrospinning Set-up

4.3.3. Morphology

The morphology of the electrospun nylon-6 webs was observed by scanning electron microscopy (SEM) using a JEOL JSM-6400 FE with Energy Dispersive X-ray Spectroscopy (EDS) operating at 5 kV. The electrospun samples were coated with Au/Pd using a K-550X sputter coater of 100 Å thickness to reduce charging. Diameter and void space of the electrospun nylon-6 mats were measured with Image J analysis software.

4.3.4. Interfacial and Viscosity Measurements

An automated contact angle goniometer (Rame-Hart, Inc., Mountain Lakes, NJ) used for data collection and calculations in combination with the DROPimage computer program. The capillary drop was formed within an environmental chamber at room temperature, in which standing water increased the relative humidity to minimize evaporation effects. An illustration of the instrument is shown in Fig. 2. It consists of a goniometer fitted with a macro lens and autobellows (Olympus) and a CCD video camera. The video frames are captures by a DT3155 frame grabber (Data Translation) in a Pentium 200 PC. The drop control unit is a Microlab M dispenser (Hamilton) and a specially designed oscillation unit consisting of a syringe with an excenter-mounted piston that is motor driven. The dispenser is controlled by the PC. The dispenser and oscillation units are mounted in series with stainless steel pipes that are filled with distilled water. The drops and bubbles are extended from the tip of a small Teflon tube into a quartz cuvette inside a thermostated and water-filled environment chamber with glass windows. The Teflon tube contains an air pocket toward the water in the steel pipe.

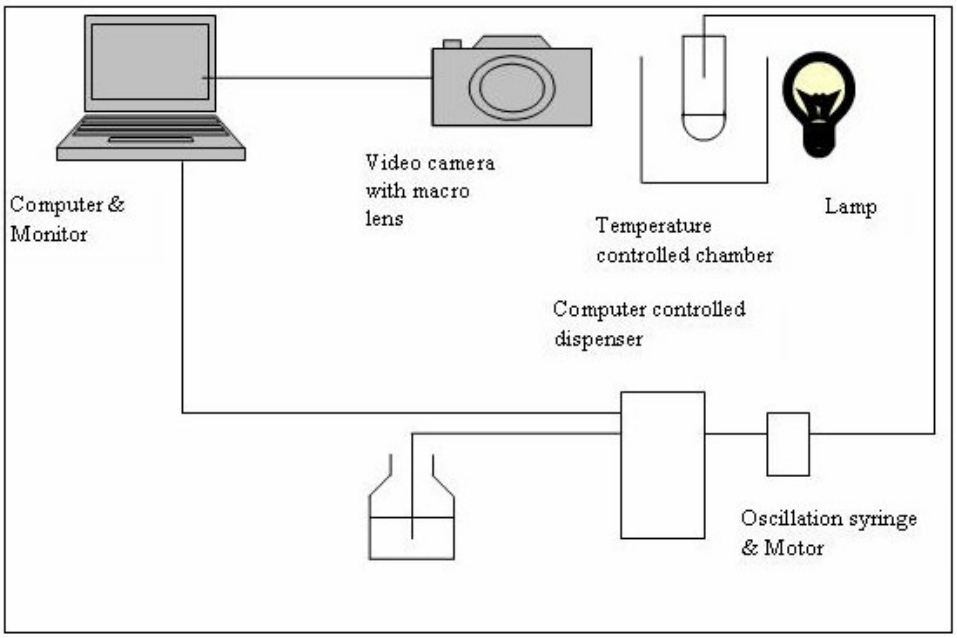

Figure 2: DROP instrument for the measurement of interfacial tension [34]

The results that are calculated are the surface tension, shape factor (b), radius of curvature (R_0), the drop volume, height and width, the surface area, and the contact angle with the horizontal plane. The surface tension of the monolayers is measured by means of a Wilhelmy plate [31].

Viscosity was measured using a rheometer (StressTech HR, Rheologica Instruments AB) with rheoExploer V5 operating software using concentric cylinder geometry as the samples were more fluidic. Samples were presheared at 30 Pa for 60 sec and all experiments were performed at 25 ºC.

4.3.5. Mechanical properties measurements

The MTS tensile tester was used for measuring tensile properties of electrospun web. ASTM D882 method of testing was used for the nonwoven electrospun nylon-6 mats.

The gauge length of the mats was 3 cm and average thickness was 0.14 mm. Tensile properties of electrospun web were measured with 10 mm/min strain rate. Void volume fraction was calculated using Image J analyzer. SEM images were scanned and different layers of nanofibers were made distinct using a grey scale. The void area (proportional to volume) was calculated as area of single nanofiber layer subtracted from total area in that plane.

4.4. Results and Discussion

4.4.1. Effect of molecular weight and concentration on surface tension

It is well known that the morphology of electrospun fibers depends on the processing parameters and environmental conditions such as temperature and humidity [7-8, 17-18]. The optimal electrospinning conditions for the three nylons (the parameters such as polymer concentration, applied electric field strength and tip-to-collector distance) were examined. The viscosity, net charge density and surface tension of solution are key parameters of the formation of the stabilized jets [19]. For low and medium molecular weight nylon-6 (at 10 wt % concentration) the solution viscosity (can be controlled by the solution concentration) was too low to make fibers. Surface tension of the low, medium and high molecular weight nylon-6 with two concentrations (10 & 15 wt %) was measured. At 10 wt % concentration, surface tension almost remains constant among high, medium and low molecular weight nylon-6, however slight difference was noticed at the concentration of 15 wt %. The results of Table 3 show that with increasing molecular weight and concentration, change in surface tension is insignificant where as, viscosity increases appreciably as shown in Table 4. Surface tension therefore, is not as

sensitive to molecular weight and concentration of polymer in electrospinning as viscosity. Polymer solutions are essentially non-Newtonian fluids, elongational flow resists the break up of the viscoelastic jet, leading to the formation of long threads of mini jets. As a result, morphology of nanofibrous structures has a dependence on these two factors (Mw and concentration). Hence, polymer concentration and molecular weight have tremendous effect on the viscoelastic jets of nanofibers [32].

Table 3: Surface tension (mN/m) of nylon-6 solutions in formic acid at different molecular weight and concentration

Concentration	**LMW**	**MMW**	**HMW**
10 wt %	**40.16±0.04**	**40.17±0.01**	**40.19±0.05**
15 wt %	**40.15±0.03**	**41.35±0.01**	**41.63±0.01**

Table 4: Variation in viscosity as a function of molecular weight and concentration.

Molecular Weight (gm/mol)	**Concentration**	**Viscosity (cP)**
LMW	10 wt %	29.6
HMW	10 wt %	53.1
LMW	15 wt %	129
HMW	15 wt %	154

4.4.2. Effect of Concentration and Molecular Weight on morphology of nanofibers

Assessment of scanning electron micrographs of three nylon-6 molecular weights revealed effect of concentration on the nanofiber morphology as shown in Figure 3. For low and medium molecular weight nylon-6 no nanofibers are observed at 10 wt. % concentration. This is attributed to the low viscosity resulting in low viscoelastic force due to low degree of chain entanglement not able to withstand the applied electric field. A study on role of chain entanglements during electrospinning has been done by Shenoy et al. [41]. This is given by the equation:

$$(\eta_e)_{sol} = \varphi_p M_w / M_e \quad (3)$$

Where $(\eta_e)_{sol}$ is the solution entanglement number, φ_p is volume fraction of polymer in solution, M_w is weight average molecular weight of polymer and M_e is entanglement molecular weight of polymer. (M_e for nylon-6 is 5000 gm/mol [42]). Based on above equation $(\eta_e)_{sol}$ was calculated and is shown in Table 5. We observe that as the value of $(\eta_e)_{sol}$ approaches 2, fiber formation is seen.

Table 5. Estimation of solution entanglement number for different nylon-6 solutions [40]

Molecular weight	**Concentration (wt %)**	**$(\eta_e)_{sol}$**
30000	10	0.634
30000	15	0.948
50000	10	1.05
50000	15	1.58

Table 5 Contd.

63000	10	1.33
63000	15	1.99

Jet stability is an important factor in formation of nanofibers. Under high electric fields in the case of 10 wt % concentration of low and medium molecular weight nylon samples, jet stability is not achieved, and as a result it breaks into smaller jets and form beads. High molecular weight nylon-6 sample at same concentration showed nanofibers relatively higher in number in contrast to low and medium molecular weight with fewer beads. At 15 wt % concentration, low and medium molecular weight nylons formed beaded and broken nanofibers whereas high molecular weight nylon produced bead free nanofibers. Therefore, as the concentration and molecular weight increases, occurrence of beads decreases. This is due to the increased degree of chain entanglement with the rise in molecular weight ultimately causing an increase in viscosity and therefore higher viscoelastic force causing elongation of fibers. Figure 3 shows that in all the samples, an increase in concentration resulted in formation of nanofibers. A reduction in average bead size was also seen. For example, the average bead size reduced from 433.54 nm to 129.2 nm and the number of beads reduced from 0.465/μm^2 to 0.09/μm^2 in the case of high molecular weight nylon-6.

Viscosity increases due to increase in molecular weight as number of chain entanglements increase. As a result, the viscoelastic forces in the polymer solution rise, so much so that the viscoelastic forces are able to counter the electrostatic force and surface tension thus producing continuous nanofibers. Elasticity of polymer solution is

vital in the study of the elongational flow characteristics. The longest relaxation time (λ) of the molecules in solution can be estimated from the Rouse model [33-34]

$$\lambda \approx 6\,\eta_s\,[\eta]\,M_w/\pi^2 RT \qquad (4)$$

where η_s is the solvent viscosity, [η] is the intrinsic viscosity, R is the gas constant and T is the temperature. An increase in molecular weight increases the relaxation time of the polymer. The relaxation time of low, medium and high molecular weight polymer (from equation 4) is calculated as 1.65 x 10^{-2}, 3.35 x 10^{-2} and 5.48 x 10^{-2} sec respectively. Its evident that with an increase in molecular weight the relaxation of polymer chains becomes more difficult and as a consequence, the elongational flow is reduced and we get nanofibers with larger diameters. At 15 wt % concentration, high molecular weight nylon-6 shows smooth and uniform nanofibers whereas medium and low molecular weight nylon-6 shows beaded nanofibers Fig. 3 (b, e & f). Hence, as the molecular weight increases, tendency to form nanofibers also increases. Similar phenomenon is observed in all the samples with an increase in concentration. Comparison of 15 wt. % high and medium molecular weight nylon-6 in Fig. 4 shows that average diameter of nanofibers increases with increasing molecular weight. The diameter distribution of high molecular weight is narrower than that for medium molecular weight.

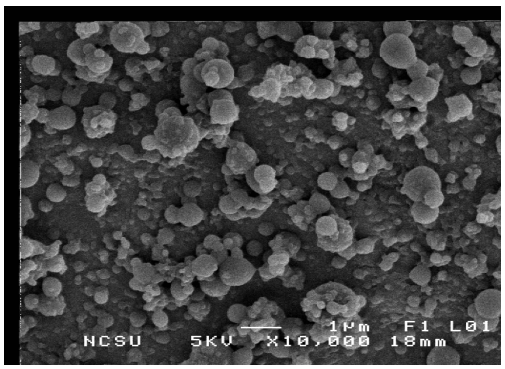

Fig 3 a. $LMWC_1V_2F_1D_2$

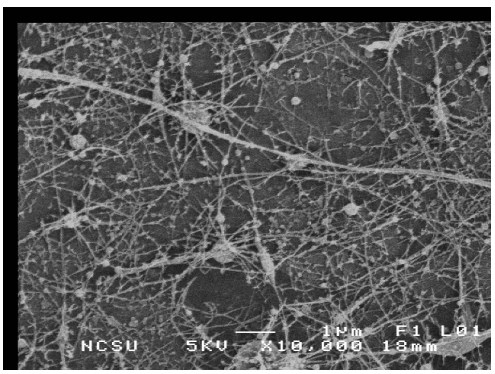

Fig 3 b. $LMWC_2V_2F_1D_2$

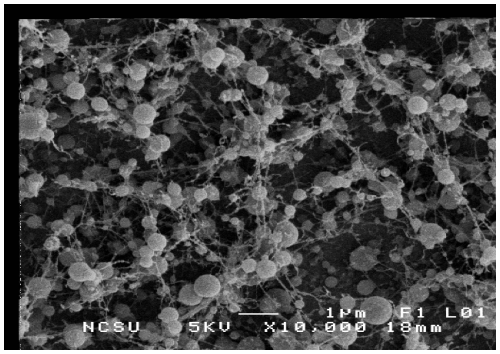

Fig 3 c. $MMWC_1V_2F_1D_2$

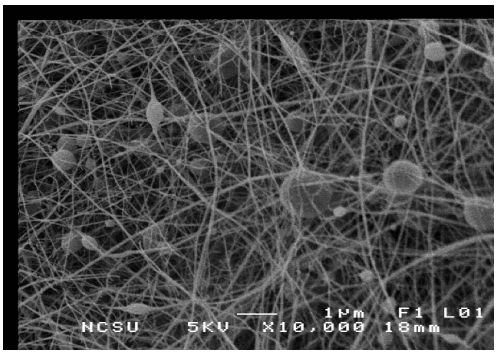

Fig 3 d. $MMWC_2V_2F_1D_2$

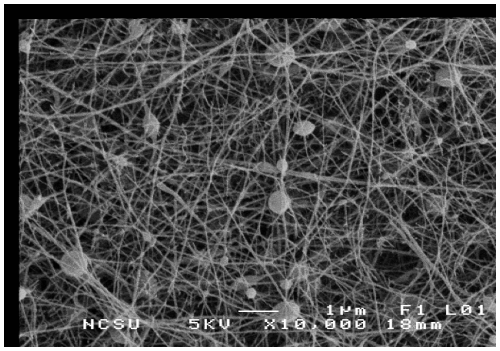

Fig 3 e. $HMWC_1V_2F_1D_2$

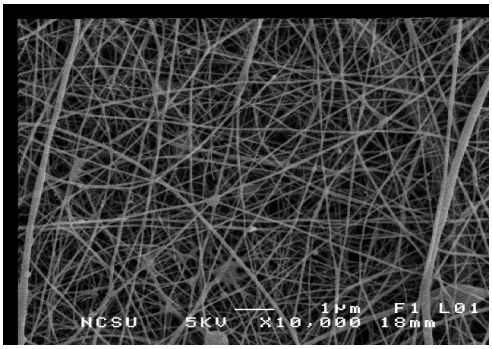

Fig 3 f. $HMWC_2V_2F_1D_2$

Figure 3: Effect of molecular weight and concentration on morphology of nanospun fibers. Low Mw nylon-6 10 wt % (a) & 15 wt % (b); Medium Mw nylon-6 10 wt % (c) & 15 wt % (d); high Mw nylon-6 10 wt % (e) & 15 wt % (f) (All samples at 15kV, 15 µl/min, 15 cm)

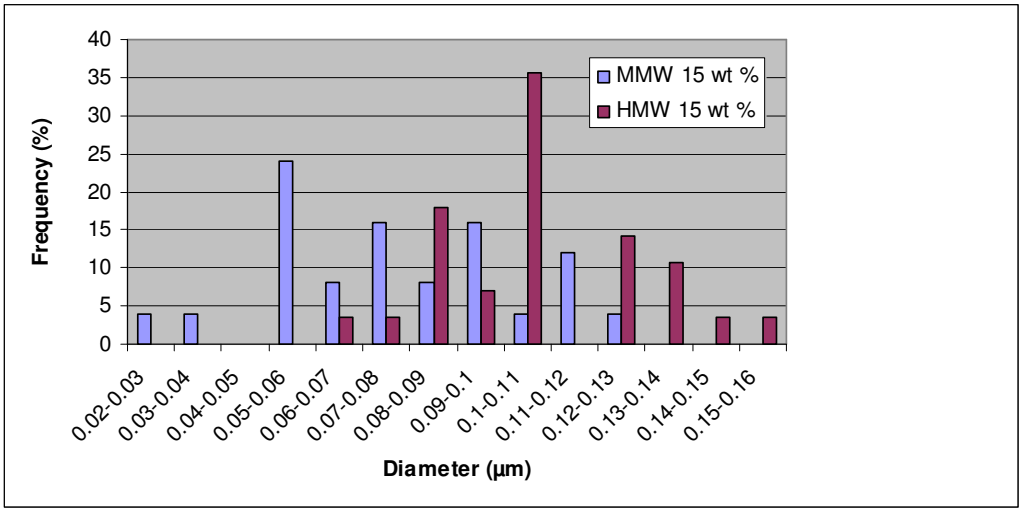

Figure 4: Effect of molecular weight on diameter distribution

4.4.3. Effect of Voltage on morphology of nanofibers

Voltage illustrates enormous effect on morphology of nylon-6 nanofibers as shown by the SEM micrographs in Figure 5. Three voltages were selected 10, 15 and 20 kV at which nanofibers were produced. For a particular molecular weight, other parameters such as concentration, distance and feed rate were kept constant at 15 wt %, 15 cm and 15 μl/min respectively.

As shown in Fig. 5 for the low and medium molecular weight nylon samples, as the voltage was increased from 10 kV to 20 kV a drop in bead formation was observed. In the case of low molecular weight nylon-6 sample at lower voltages of 10 and 15 kV essentially no nanofibers are seen but at 20 kV some fibers started to form. Same trend was observed for medium molecular weight sample but with higher number of nanofibers. It is evident from Figure 5 (a-f) that an increase in voltage with other parameters kept constant leads to improved nanofiber formation with a relative decrease in bead size.

For high molecular weight 15 wt % nylon-6 dissimilar results were obtained. Herein, at 10 kV the tendency of nanofiber formation seemed to be the greatest with long continuous nanofibers and diminished as the voltage was subsequently increased to 15 and 20 kV. At 20 kV no nanofibrous mat was seen, only single rope like structure was formed. It is clear that there is an optimum voltage condition characteristic of a polymer molecular weight and concentration which maximizes the whipping instability to form thin fibers. Though nanofibers from whole range of molecular weights were obtained

nevertheless, nanofibers obtained from high molecular weight nylon-6 were without beads and more uniform as compared to other samples.

We assume that increasing voltage further could furnish uniform nanofibers. Effect of voltage on the nanofiber diameter distribution demonstrates that in all the samples as the voltage is increased diameter also increases. Average diameter of nanofiber for medium molecular weight nylon-6 increased from 78 nm at 15 kV to 83 nm at 20 kV. For high molecular weight nylon-6 average diameter increased from 77.16 nm at 10 kV to 93.76 nm at 15 kV. Figure 6 (a, b) shows the diameter distribution as a function of voltage. The rationale behind this observation is that an increase in voltage drives the charged jet to emerge from tip through Taylor's cone rapidly due to higher electrostatic forces, so the solvent is removed more quickly resulting an increase in fiber diameter. These results agree with work carried out by Zhang and co-workers [35].

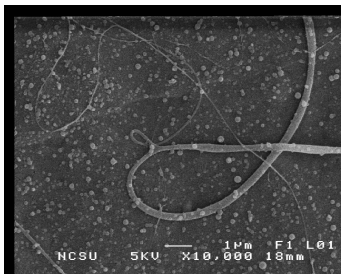

Fig 5 a. $LMWC_2V_1F_1D_2$

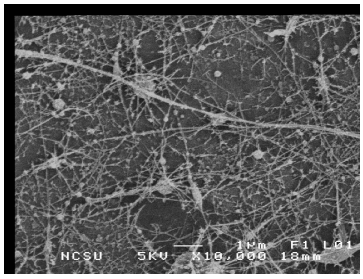

Fig 5 b. $LMWC_2V_2F_1D_2$

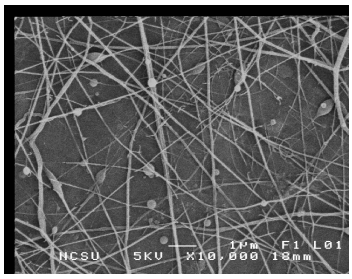

Fig 5 c. $LMWC_2V_3F_1D_2$

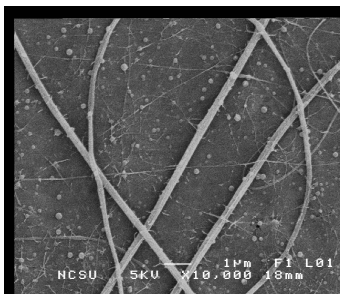

Fig 5 d. $MMWC_2V_1F_1D_2$

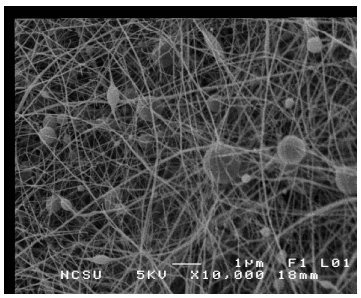

Fig 5 e. $MMWC_2V_2F_1D_2$

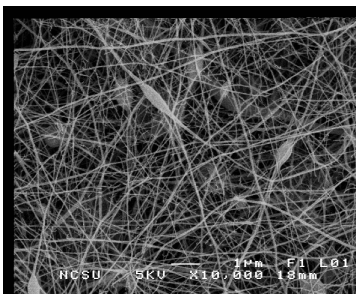

Fig 5 f. $MMWC_2V_3F_1D_2$

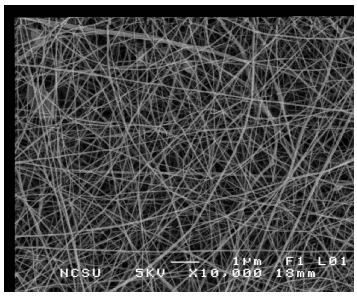

Fig 5 g. $HMWC_2V_1F_1D_2$

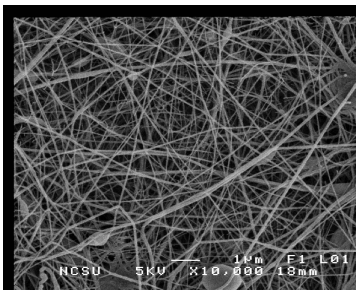

Fig 5 h. $HMWC_2V_2F_1D_2$

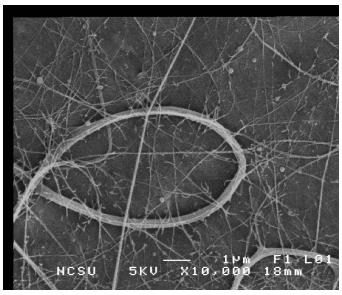

Fig 5 i. $HMWC_2V_3F_1D_2$

Figure 5: Effect of Voltage

(a, b, c) Low Mw nylon-6 at 10, 15, 20 kV; (d, e, f) Medium Mw nylon-6 at 10, 15, 20 kV; (g, h, i) High Mw nylon-6 at 10, 15, 20 kV (All samples at 15 wt%, 15 µl/min, 15 cm)

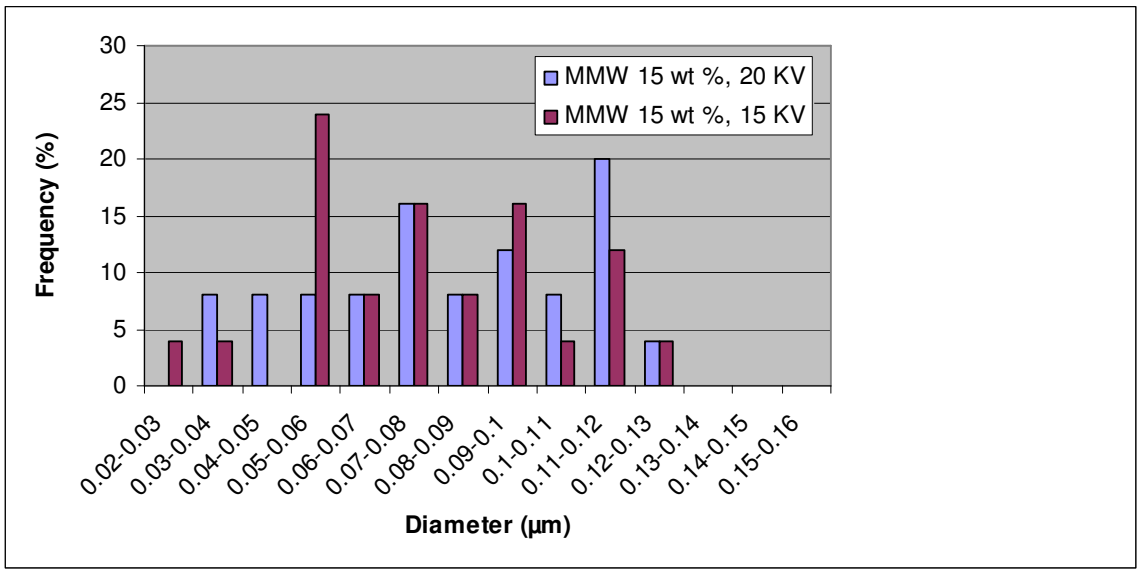

Figure 6 (a)

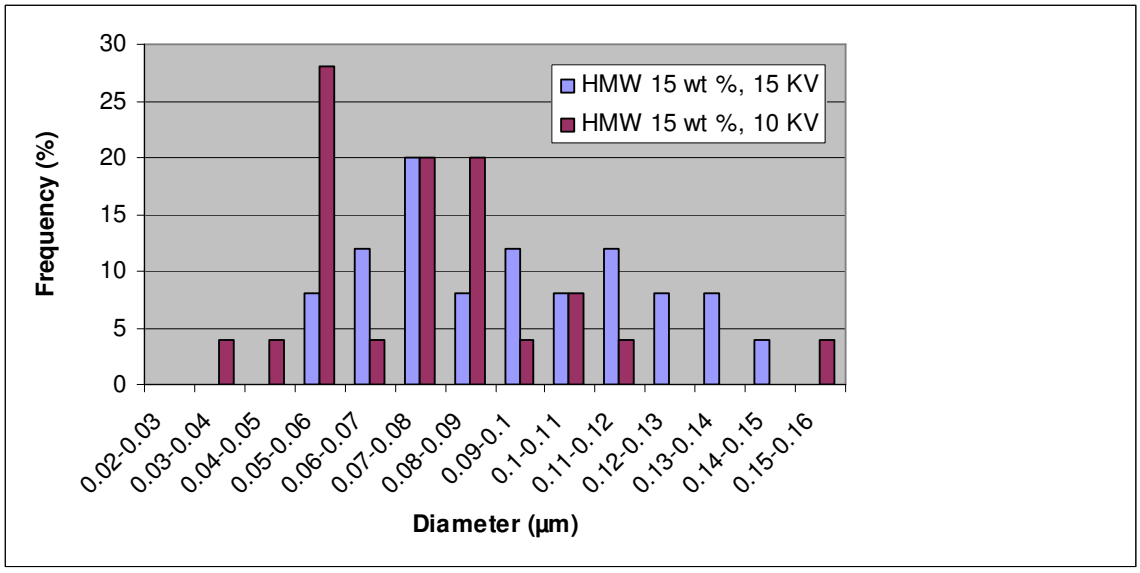

Figure 6 (b)

Figure 6 (a, b): Diameter distribution as a function of voltage. Increase in voltage augmented diameter size in medium Mw (Fig 6a) and high Mw (Fig 6b) nylon-6.

4.4.4. Effect of Distance on morphology of nanofibers

The distance between the tip of the capillary and the grounded plate can have a significant impact on morphology of electrospun nanofibers. Three different distances were chosen 10, 15 and 20 cm between the tip of the needle and the grounded plate. For a particular molecular weight, other parameters such as concentration, voltage and feed rate were kept constant at 15 wt %, 15 kV and 15 µl/min, respectively.

As the distance between the tip and grounded plate increased, more uniform and beadless nanofiber were obtained in all nylon-6 samples. For example, Fig 7 shows the trend observed in the case of low molecular weight nylon-6 (15 wt %). We see that as the distance increased from 10 to 20 cm, a progressive reduction in bead occurrence is

observed, same result was observed in the case of medium and high molecular weight samples. An increase in distance provides more time for solvent evaporation, resulting in finer nanofibers and uniform diameter size. High molecular weight 15 wt % nylon-6 was also electrospun at a distance of 20 cm. Figure 7 (c, d) shows that high molecular weight 15 wt % nylon-6 showed more consistent nanofibers as compared to low molecular weight 15 wt %. We observed that there is a difference in the morphology of the nanofibers from two samples at similar conditions, low molecular weight sample are less uniform with more beads as compared to high molecular weight nylon-6 as predicted by Shenoy [41] based on entanglement concentration.

Figure 8 quantitatively shows that in case of low molecular weight nylon-6 that as distance increases the diameter of nanofibers decreases. Average diameter decreased from 78.52 nm to 64.92 nm

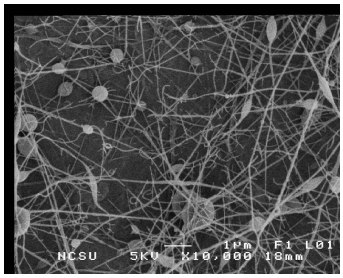

Fig 7 a. $LMWC_2V_2F_1D_1$

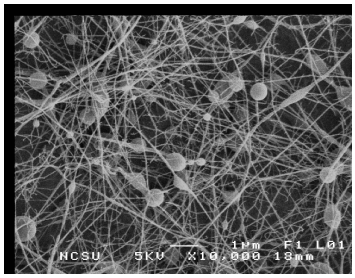

Fig 7 b. $LMWC_2V_2F_1D_2$

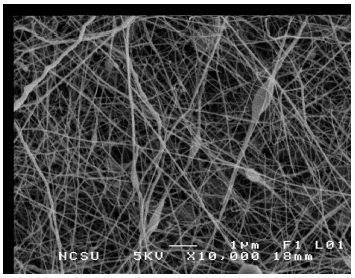

Fig 7 c. $LMWC_2V_2F_1D_3$

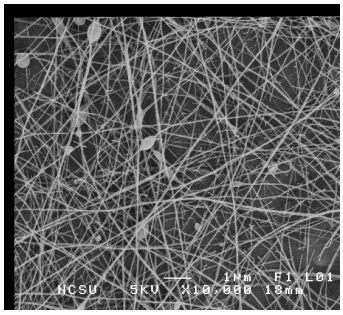

Fig 7 d. $HMWC_2V_2F_1D_3$

Figure 7: Effect of distance on nanofiber morphology.

(a, b, c) Low Mw 15 wt % nylon-6 at distance 10, 15 and 20 cm. (d) high Mw 15 wt % nylon-6 at distance 20 cm (All samples at 15 KV, 15 µl/min)

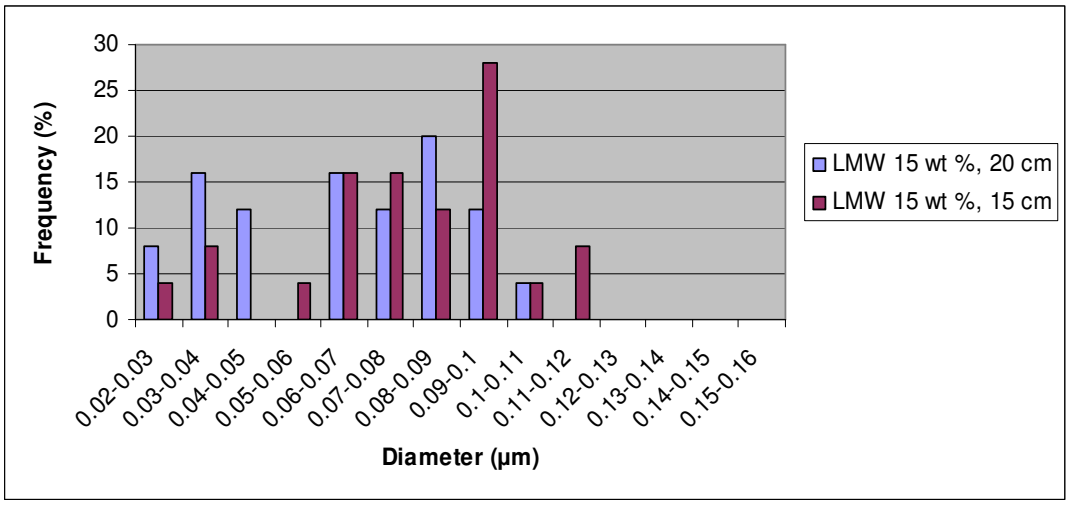

Figure 8: Diameter distribution as a function of distance and molecular weight.

4.4.5. Effect of Feed Rate on morphology of nanofibers

Three feed rates were chosen to determine the effect of mass throughput (15, 50 and 100 µl/min) on fiber morphology. Other parameters such as concentration, voltage and distance were kept constant at 15 wt %, 15 kV and 15 cm respectively. The general trend depicted an increase and then decrease in fiber forming tendency as the feed rate was progressively increased.

At 15 wt % concentration, medium molecular weight nylon-6 was chosen to ascertain the effect of varying feed rate. Nanofibers with typical beads on string structure were observed at 15 µl/min. When the feed rate was increased to 50 µl/min, frequency of beads declined and more slender nanofibers were noticed. Finally, at a rate of 100 µl/min, no nanofibers were formed, instead a thick rope like structure was seen (Fig. 9 a,b,c). At 15 wt % concentration similar results were seen for high molecular weight nylon-6. As the feed rate was increased from 15 to 100 µl/min, morphology shifted from un-beaded nanofibers to non-uniform nanofibers with beads (Fig. 9 d,e,f). At 10 wt % concentration high molecular weight nylon-6 gave analogous results which further verify our earlier results (Fig. 9 g,h). As the feed rate increases, more polymer is available at the needle tip to be electrospun which exceeds the rate of removal at a fixed electric field and therefore this mass imbalance gives rise to beaded or thick nanofibers.

A careful look on the diameter distribution in Figure 10 shows that as the feed rate was increased, the average diameter increased from 67.64 nm to 123.28 nm as the feed rate

was increased from 15 to100 µl/min in the case of high molecular weight (15 wt %) nylon-6.

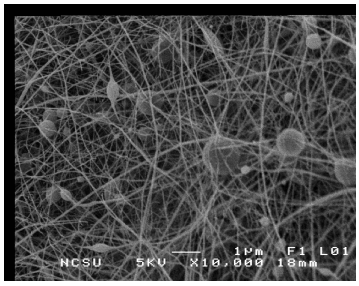

Fig 9 a. $MMWC_2V_2F_1D_2$

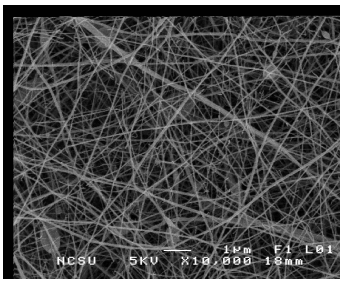

Fig 9 b. $MMWC_2V_2F_2D_2$

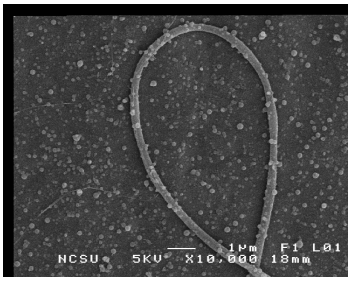

Fig 9 c. $MMWC_2V_2F_3D_2$

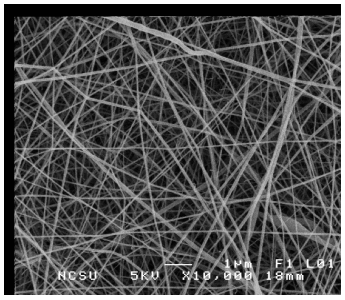

Fig 9 d. $HMWC_2V_2F_1D_2$

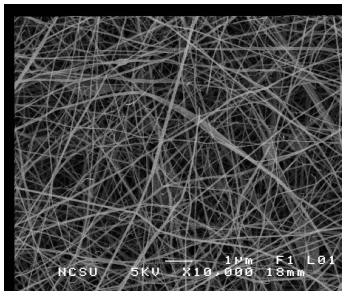

Fig 9 e. $HMWC_2V_2F_2D_2$

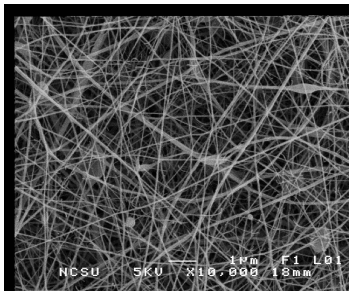

Fig 9 f. $HMWC_2V_2F_3D_2$

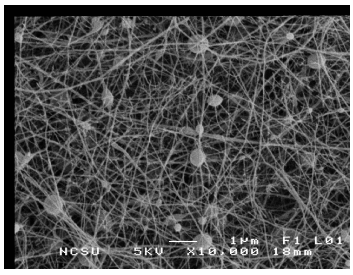

Fig 9 g. $HMWC_1V_2F_1D_2$

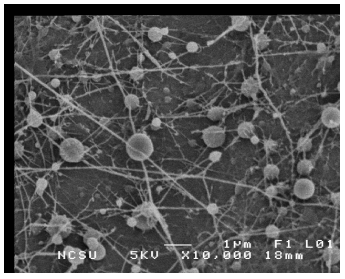

Fig 9 h. $HMWC_1V_2F_2D_2$

Figure 9: Effect of Feed Rate

(a, b, c) Medium Mw 15 wt % nylon-6 at 15, 50, 100 µl/min; (d, e, f) High Mw 15 wt % nylon-6 at 15, 50, 100 µl/min; (g, h) High Mw 10 wt % nylon-6 at 15 and 50 µl/min (All samples at15 wt%, 15 KV, 15 cm)

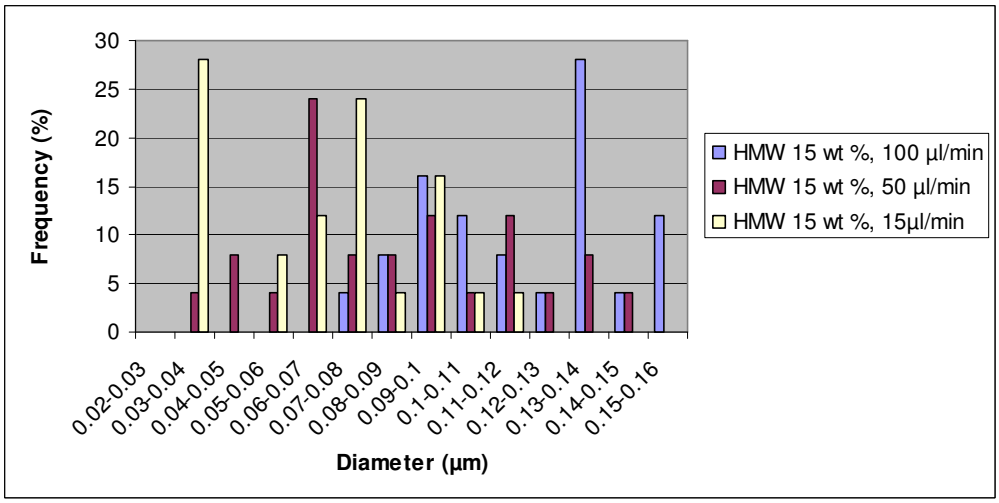

Fig 10 (a)

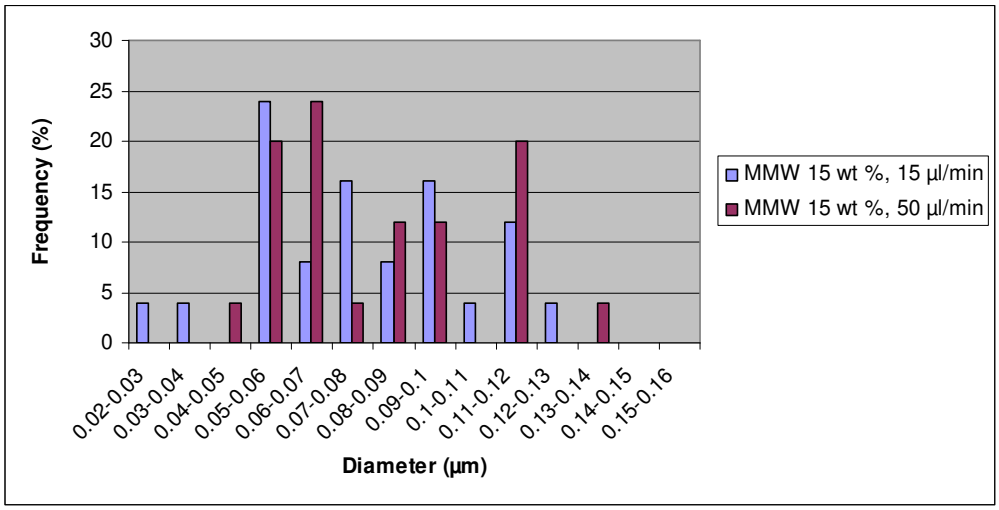

Fig. 10 (b)

Figure 10 (a, b) Effect of Feed rate on diameter distribution on high Mw (Fig 10 a) and medium Mw (Fig 10 b) shows an increase overall diameter size with an increase in feed rate.

4.4.6. Mechanical Testing of Nanofibrous mats

As the molecular weight of a polymer increases, mechanical properties also increase due to increased number of chain entanglements. However, it is unclear what the effect of

Mw has on the mechanical properties of the fibrous mat would be, since the mechanical properties are dependent on both fiber properties as well as the bond strength of fiber-fiber junctions. As Mw increases we expect fiber strength/modulus to increase, however we are unsure of the effect Mw will have on the strength of the fiber-fiber weld points. (We would expect the interdiffusion to decrease as Mw increases, but are unsure of how that will effect the weld strength).

Our mechanical test results proved that as the molecular weight increased, modulus of nonwoven electrospun nanofiber mats increased. The tests were performed on nanofibrous electrospun mats having identical processing conditions like feed rate, tip to grounded plate distance electric field and each of the experiments were timed so as to keep the thickness of mats uniform. Five samples of each molecular weight were tested for statistical purposes. These results account for the porosity of the mats and void volume fraction was measured using Image J software. The void volume fraction for high, medium and low molecular weight nylon-6 samples was calculated as 84.6, 86.8 and 86 % respectively. Table 6 shows that Young's modulus increased almost 50 % as a function of increasing molecular weight. Tenacity also showed an increase as Mw increased. Therefore Mw did not have an adverse effect on the strength of the fiber-fiber junctions (within the Mw range studied).

Table 6. Tensile properties of electrospun nylon-6 web

Electrospun web	Tenacity (kgf)	Elongation at break (%)	Modulus (kgf/mm^2)
HMW	0.4 ± 0.07	16.6 ± 2.5	5.1 ± 0.59
MMW	0.312 ± 0.019	18.65 ± 0.75	4.37 ± 0.59
LMW	0.15 ± 0.02	9.3 ± 1.7	3.26 ± 0.21

4.5. Conclusion

In the present endeavor, the electrospinning technique was used to produce nanoscale fibers of nylon-6. The core objective of this study was to fabricate nanofibers of high molecular weight of nylon-6 for understanding entanglement of linear polymer chains and its effect on morphology and jet stability of electrospun fibers. To substantiate our study it was necessary to probe low and medium molecular weight nylon-6 and compare with the high molecular weight nylon-6. Variation in surface tension was insignificant with an increase in molecular weight and concentration of polymer. Molecular weight and concentration are prime factors affecting the morphology of the nanofibers. At same concentration level, low molecular weight nylon-6 formed small droplets, while medium molecular weight fibers just started to form nanofibers but high molecular weight nylon-6 formed mats of nanofibers. An increase in relaxation time (as molecular weight increases) suppresses the jet instability due to increased chain entanglements, forming unbeaded and continuous fibers.

Variation in voltage has strong effect on the morphology on nanofibers. With an increase in voltage more fibers are formed with less beads and larger diameters. For high

molecular weight nylon-6 it was possible to manufacture nanofibers even at low voltages as against low and medium molecular weight nylon-6. With an increase in tip to collector distance, (thereby increasing the time of flight of nanofibers), a reduction in diameter size is observed. The diameter of electrospun nanofibers increased with an increase in feed rate. Favorable feed rate to produce nanofibers was higher in case of low molecular weight and lower in case of high molecular weight nylon-6. Mechanical properties showed that tenacity as well as modulus increase as molecular weight is increased with no negative effects on the fiber-fiber weld points.

4.6. Acknowledgements:

We gratefully acknowledge Dr. Dale Batchelor for kindly helping and providing us SEM micrographs. We are thankful to Dr. Brian E. Farkas and Paige Luck for helping us in Surface Tension measurements and Jamal Irving for contributing efforts in research.

4.7. References

1. Huang-Zhang, Y. Z.; Kotaki, M.; Ramakrishna, S. Composites Science and Technology 2003, 63, 2223.
2. Pedicini, A.; Farris, R. J. J Polym Sci Nylonrt B: Polym Phys 2004, 42, 752.
3. Deitze, J. M.; Kosik, W.; McKnight, S. H.; Beak-Tan, N. C.; Desimone, J. M.; Crette, S. Polymer 2002, 43, 1025.
4. Ding, B.; Kim, H. Y.; Lee, S. C.; Shao, C. L.; Lee, D. R.; Park, S. J.; Kwag, G. B.; Choi, K. J. J Polym Sci, Part B: Polym Phys 2002, 40, 1261.
5. Dai, H.; Gong, J.; Kim, H. Y.; Lee, D. R. Nanotechnology 2002, 13, 674.
6. Deitzel, J. M.; Kleinmeyer, J.; Harris, D.; Beck-Tan, N. C. Polymer 2001, 42, 261.
7. Reneker, D. H.; Chun, I. Nanotechnology 1997, 7, 216.
8. Bergshoef, M. M.; Vancso, G. J. Adv Mater 1999, 11,362.
9. Doshi, J.; Renker, D. H. J Electrostat 1995, 35, 151.
10. Gibson, P. W.; Schreuder-Gibson, H. L.; Riven, D. AIchE J 1999, 45,190.
11. Fong, H., Renker, D. H. Structure formation in polymeric fibers', In Salem, D. R.; Sussman, M. V., Editors. Electrospinning and formation of nanofibers; Hanser: Munich, 2001, Chapter 6.
12. Hou, H.; Jun, Z.; Reuning, A.; Schaper, A.; Wendorff, J. H.; Greiner, A. Macromolecules 2002, 35, 2429.
13. Kenawy, E. R.; Bowlin, G .L.; Mansfield, K.; Layman, J.; Simpson, D. G.; Sanders, E. H. Journal of Controlled Release 2002, 81,57.
14. Scopelianos, A. G. US Patent, 5522879, 1996.

15. Larrondo, L.; Manley, R. J Polym Sci Part B: Polym Phys 1981, 19, 921.
16. Fong, H.; Chun, I.; Renker, D. H. Polymer 1999, 40, 4585.
17. Bognitzki, M.; Czado, W.; Frese, T.; Schaper, A.; Hellwig, M.; Steinhart, M.; et al. Adv Mater 2001, 13, 70.
18. Lee, K. H.; Kim, Y. H.; La, Y. M.; Lee, D. R.; Sung, N. H. J Polym Sci Part B: Polym Phys 2002, 40, 2259.
19. Zuo, W.; Zhu, M.; Yang, W.; Yu, H.; Chen, Y.; Zhang, Y. Polym Eng Sci 2005, 45, 704.
20. Zimmerman, J.; Mark, H. F.; Bikales, N. M. In: Encyclopedia of polymer science and engineering; Wiley: New York, Vol. 6, 1988, 802.
21. Ziabicki, A. Fundamentals of fiber formation: The science of fiber spinning and drawing; Wiley: New York, 1976.
22. Ryu, Y. J.; Kim, H. Y.; Lee, K. H.; Park, H. C.; Lee, D. R. Eur Polym J 2003, 39, 1883.
23. Fong, H.; Liu, W.; Wang, C.; Vaia, R. A. Polymer 2002, 43, 775.
24. Larrondo, L.; Manley, R. J Polym Sci Part B: Polymer Physics 1981, 19, 933.
25. Schreuder-Gibson, H. L., Gibson, P., Senecal, K., Sennett, M., Walker, J., Yeomans, W. Journal of Advanced Materials 2002, 34, 44.
26. Stephen, J. S.; Chase, D. B.; Rabolt, J. F. Macromolecules 2004, 37, 877.
27. Supaphol, P.; Upnylontham, C. M.; Nithitanakul, M. J Polym Sci Part B: Polymer Physics 2005, 43, 3699.
28. Uppatham, C. M.; Nithitanakul, M.; Supaphol, P. Macromolecular Chemistry and Physics 2004, 205, 2327.

29. Supaphol, P.; Uppatham, C. M.; Nithitanakul, M. Macromolecular Materials and Engineering 2005, 290: 933.

30. Dersch, R.; Liu, T.; Schaper, A. K.; Greiner, A.; Wendorff, J. H. J Polym Sci Part A: Polymer Chemistry 2003, 41, 545.

31. Myrvold, R., Hansen, F. K. J. Colloid Interface Sci. 1998, 207, 97.

32. Mun, R. P.; Byars, J. A.; Boger, D. V. Journal of Non-Newtonian Fluid Mechanics 1998, 74, 285.

33. Sperling, L. H. Introduction to Physical Polymer Science, 2nd Ed.; Wiley: New York, 1992.

34. Koski, A.; Yim, K.; Shivkumar, S.; Mat. Lett. 2004, 58, 493-497.

35. Zhang, C., Yuan, X., Wu, L., Han, Y., Sheng, J. European Polymer Journal 2005, 41, 423

36. Bandrup, J.; Immergut, E. H. Polymer Handbook, Wiley: New York, 1975.

37. Srinivasan, G.; Reneker, D. H. Polymer Int 1995, 36, 195

38. Fang, X., Reneker, D. H. Journal of Macromol Sci Phy 1997 B 36 (2), 169.

39. Fong, H.; Reneker, D. H. J Polym Sci Part B: Polym Phys, 1999, 37, 3488.

40. Larrondo, L.; Marley, R. J. Polym. Sci. Part B: Polym Phys 1981, 19, 909.

41. Shenoy, S. L.; Bates, W. D.; Frisch, H. L.; Wnek, G. E. Polymer 2005, 46, 3372.

42. Zang, Y. H.; Carreau, P. J. J Appl Polym Sci 1991, 42, 1965.

Chapter 5

Fabrication and characterization of chitosan nanofibers produced by bi-component electrospinning

*Satyajeet S. Ojha[1], Derrick R. Stevens[2], Torissa J. Hoffman[2], Rebecca Klossner[1], Laura I. Clarke[2], Wendy Krause[1] and Russell E. Gorga[1]**
[1]Department of Textile Engineering, Chemistry and Science, NCSU, [2]Department of Physics, NCSU

5.1. Abstract:

Chitosan is a naturally occurring polysaccharide, biocompatible and recognized as an antibacterial agent. As an abundantly common biopolymer, chitosan has been extensively discussed as a material for formation of artificial tissue scaffolds. In order to match the morphology of mammalian extracellular matrices, such scaffolds require high porosity (>70%) and fiber diameters ≤ 100 nm, morphology that can be obtained from mats of electrospun fibers.. Past attempts to electrospin chitosan have utilized polymer blends. Here, Polyethylene oxide (PEO) has been used as a template to fabricate chitosan nanofibers which is complicated to form nanofibers on its own. 3 wt % chitosan as core formed coaxial nanofibers with 4 wt % PEO. Transmission electron microscopy confirmed formation of core-sheath structures. Subsequently, PEO was removed by washing with de-ionized water to obtain chitosan nanofibers. Scanning electron micrographs demonstrated development of chitosan nanofibers. Transmission electron microscopy confirmed formation of core-sheath structures. Mechanical testing of core-sheath nanofibers showed elongation at break at 14.8 % and a modulus of 2.40 kgf/mm^2. Electrical measurements on mats of core-sheath nanofibers showed no conductivity due to the presence of the insulating PEO sheath, which prevents fiber-electrode and fiber-

fiber contact. Upon removal of the sheath, mats of the chitosan nanofibers and drop-cast films of chitosan did not differ in conductivity with values of 10^{-12} - 10^{-11} S/cm in vacuum and ~10^{-9} S/cm at ambient conditions, consistent with literature precedents (on films). Upon soaking with water, which should provide the maximum conductivity, films showed a rise in conductivity to ~ 10^{-4} S/cm; however, repeated measurements on films and mats were hindered by the inability of the mat/film to swell when adhered to the surface of an electrode.

Keywords: coaxial electrospinning, polysaccharide, scaffolds.

5.2. Introduction:

Electrospinning is a technique which has gained momentum in the recent past to generate fibers at the sub-micron scale.[1-4] The electrospinning process yields nanofibers with a 3-D porous network with ultra high aspect ratio and enormous specific surface area which makes them useful in fields like drug delivery[2], tissue engineering[6], conductive nanowires[7], super-capacitors[8], nanosensors[9], wound dressings[10] and filtration membranes.[11-12] Due to its versatility in applications, an abundance of polymers have been electrospun into nanofibers.[5]

In electrospinning, a non-mechanical process, electrical forces are used instead of mechanical forces to produce fibers.[13] In a typical electrospinning set-up, a polymer solution or melt in a syringe is charged through a high voltage supply and a grounded

plate is placed at a fixed distance form the needle tip. Due to the large potential difference, the fluid droplet at tip of the metal needle (used in conjunction with syringe) overcomes surface tension thereby forming jet of nanofibers by the action of electric Maxwell stresses.[14] Hohman et.al.[15] has modeled the role played by surface charge in suppressing the Rayleigh instability and boosting whipping instability which results in stretching of the jet. The grounded electrode in the form of circular plate, rotating drum or parallel bars is placed for deposition of nanofibers.[16] Morphology of nanofibers obtained from electrospinning depends upon both the solution parameters such as viscosity, surface tension, charge density[17] and processing variables like applied voltage, tip to collector distance, feed rate, humidity and temperature.[18-20]

The nanofibrous mats produced by electrospinning have highly porous dense network of nanofibers with extraordinary surface area. Such properties combined with minute length scale make nanofibers advantageous to be used as a scaffolding material mimicking extra cellular matrix (ECM).[21] Bhattarai was able to show that a mixture of 80/20 Poly (L-lactic acid) (PLLA) and Poly ethylene glycol (PEG) is favorable for biological activity of NIH 3T3 fibroblast cells.[22] Collagen coated PLLA-co-Poly-(ε-caprolactore) nanofiber mesh have been used to study viability, attachment and phenotypic maintenance of human coronary artery endothelial cells (HCAECs).[23] Xin et al. demonstrated that nanofiber mesh produced by Poly (D,L-lactide-co-glycolide) (PLGA) offers accommodating milieu for human mesenchymal stem cells (hMSCs) as well as their osteogenic (hMSC-Ob) and chondrogenic (hMSC-Ch) derivatives.[24]

Recently much effort has been directed towards developing nanofibers having a core-sheath geometry. With such structure these core-sheath nanofibers could be applied to a variety of applications such as the preservation of a biological agent from externally aggressive environments and sustained delivery of drugs.[25] Electrospinning has been used as a template to prepare poly-pyrrole/poly(methyl methacrylate) coaxial nanocables,[26] fabrication of nanocables by laser ablation,[27] TUFT (tubes by fiber templates) process to produce nano-and mesocables[28] and growth of semiconductor nanowires inside polymer tubules.[29]

Coaxial electrospinning could be very helpful in cases where a particular polymer solution/melt is not capable of forming nanofibers due to its fluid characteristics. The limitation in electrospinnability of these polymers could be due to poor solubility, inappropriate molecular weight or spatial arrangement of polymer chains in solution leading to different magnitude entanglement density.[30] In this technique, two concentric needles are placed in an annular fashion, two different polymer solutions or melt or a mixture of melt or solution form a compound pendant drop at the capillary end forming a compound Taylor cone as shown in Fig.1. The two polymers do not mix since the process is very rapid.[31] For fabrication of core-sheath nanofibers, it is essential that both core and sheath fluid should be subjected to identical Maxwell stresses and bending instability.[32] A dual syringe system to produce nanofiber blends having side-by-side arrangement of syringes has also been reported.[33] Loscertales et al. have earlier shown production of core-sheath nanocapsules.[34]

Coaxial electrospinning technique was first reported by Sun et al. using two capillary spinneret using PEO-PEO (polyethylene oxide), PEO-Poly(dodecylthiphene) and PEO-polysulfone.[31] Zhang et al. demonstrated encapsulation of fluoroscein isothiocyanate-conjugated bovine serum albumin within poly caprolactone (PCL) nanofibers.[35] Similarly, encapsulation of iron-platinum (Fe-Pt) magnetic nanoparticles within PCL nanofiber has also been studied.[36] Rutledge et al. has produced polyacrylonitrile/poly (acrylonitrile-co-styrene), silk/PEO, Polyaniline/PEO core sheath nanofibers.[30,37] Li and Xia have produced core-sheath nanofiber morphology using poly (vinyl pyrrolidone)-titanium tetraisoporpoxide/mineral oil. In another attempt they presented production of Poly [2-mehtoxy-5-(2-ethylhexyloxy)-1,4-phenylvinylene] (MEH-PPV) co-electrospun with poly (vinyl pyrrolidone) as core-sheath nanofibers.[28, 38]

Chitosan ((1→4)-linked 2-amino-2-deoxy-β-D-glucan) is a linear polymer, partly deacetylated form of chitin, obtained from crustaceans. Its biocompatible, biodegradable and anti-microbial nature, has resulted in a lot of research activity in fields such as drug delivery, tissue engineering scaffold and wound healing dressings.[39-41]

Presence of amino ($–NH_2$) and hydroxyl (-OH) groups enables chitosan to be easily modified.[42-43] The end products of degraded chitosan are natural metabolites which makes it non-toxic and non-antigenic.[44] It has been estimated that 10^{10}-10^{12} tons of chitin are biosynthesized each year.[45] Molecular weight and degree of deacetylation of chitosan varies depending on the origin and method of hydrolysis.[46] Rigid D-glucosamine structures and high crystallinity, together with intermolecular hydrogen-bonds restricts

the solubility of chitosan in common organic solvents, and its tendency to form poly-ion with anionic hydrocolloids to form a gel has limited means to process chitosan.[47,48]

However attempts have been made to electrospin chitosan by blending it with other polymers such as PEO, Bhattarai et al. have used chitosan/PEO having ratio 90/10 with Triton X-100 ™ to fabricate blended nanofibers.[49] Chitosan with PEO with mass ratio 1:1 and 2:1 has been electrospun by Duan and co-workers.[50] Ohkawa et al. demonstrated fabrication of chitosan/PVA nanofibers[51]; Chitosan blended with polyacrylic acid has been reported by Chen.[52] In another technique reported by Min et al[53] chitin nanofibers were electrospun and subsequently deacetylated.

Chitosan act as wound healing accelerator and stimulates migration of inflammatory cells.[54-55] Chitosan activates macrophage which results in relaease of many growth factors such as transforming growth factor beta-1 (TGF-β1) and platelet derived growth factor (PDGF) which upregulate the ECM production.[56-57] Chitosan blended with PEO have been utilized in cartilage tissue engineering by Subramanian et al. They demonstrated that canine chondrocytes cell growth on nanofibers mats was more as compared to drop cast samples.[58] In another report, bhattarai have shown that nanofibers with high ratio of chitosan/PEO have sufficient properties such as structural integrity and adhesion for growth and proliferation of chondrocytes (HTB-94) and Osteoblast (MG-63) cells and therefore could be exploited as candidates for bone tissue engineering.[59]

In this work, we make an attempt to illustrate schematics to produce core-sheath nanofibers using chitosan and polyethylene oxide. Electrospun chitosan-PEO (core-sheath) nanofibrous mats were then subjected to de-ionized water. As a result PEO dissolves and pure chitosan nanofibers are obtained. This technique is advantageous as it provides more contact surface area of chitosan for proposed application in tissue engineering improving cell attachment and proliferation. In addition, we characterize the mechanical and electrical properties of webs of these chitosan nanofibers, with an eye to possible applications in tissue engineering. In particular, we utilize electrical conductivity tests to confirm the presence of the non-conducting sheath and to determine the conductivity of the resultant chitosan nanofibers after washing.

5.3. Experimental

5.3.1. Materials

Chitosan (82 % deacetylated) was obtained from Sigma Aldrich having a viscosity average molecular wt. of 148,000 gm/mol as calculated from the intrinsic viscosity [η] using Mark Houwink equation, $[\eta] = KM^{\alpha}$, where $K = 1.81 \times 10^{-3}$ ml/gm and $\alpha = 0.93$. The intrinsic viscosity [η] was measured in a mixture of 0.1 M acetic acid and 0.2 M sodium chloride at 25° C. Polyethylene oxide (Mw 900,000 gm/mol) was supplied by Scientific Polymers Products Inc. All samples were used without further purification. Chitosan solutions were prepared with varying concentrations (1-7 wt %) by dissolving chitosan in 90% Acetic Acid (EMD chemicals). For all the experiments concentration of PEO solution (in water) was kept constant at 4 wt %.

5.3.2. Electrospinning

Electrospinning of Chitosan/PEO solutions was performed using a horizontal set-up. A variable high voltage power supply (Glassman high voltage model # FC60R2 with positive polarity) was utilized for generating high voltage varied between 10-20 kV. Two syringe pumps (New Era NE 500), kept perpendicular to each other were used for pumping the polymer solutions at feed rates ranging from 50 to 900 µL/min. Equal mass flow rate was maintained for core and sheath polymers. Two concentric needles having diameters are 16 G and 22 G were used for sheath (PEO) and core (Chitosan) fluid respectively. Both Chitosan and PEO solution were fed from 10 mL syringes. Figure 1 shows the core-sheath electrospinning set-up.

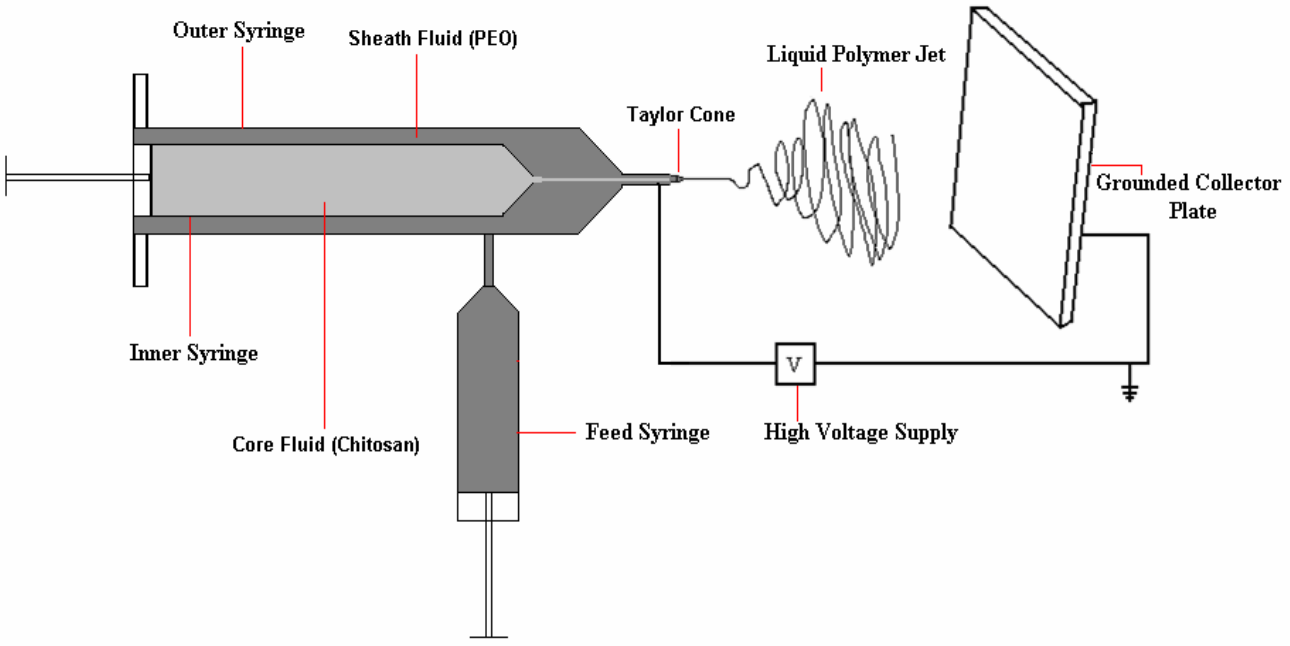

Figure 1: Typical set-up used for core-sheath electrospinning

5.3.3. Characterization

5.3.3.1. Rheology and conductivity

The StressTech HR (ATS RheoSystems, Bordentown, NJ), a stress controlled rheometer, was used to obtain the zero-shear rate viscosity (η_0). For the initial studies, a 50 mm parallel plate was used to collect the viscosity data. The gap used for all solutions was 0.300 mm at a temperature of 25°C ± 0.1°C. Additionally, to reach low shear rates with a low viscosity sample (less than 1,000 cP), a custom made double-gap, concentric cylinder geometry was used. The outer radius of the bob measures 26.22 mm, with an inner radius of 21.60 mm. A volume of 2.83 cm^3 is required for accurate measurements. This fixture allowed for precise viscosity measurements at low concentrations of chitosan. Solution conductivity was measured using Orion conductivity/salinity/temperature meter (model # 162).

5.3.3.2. FTIR

Fourier transform infrared spectroscopy was performed (Nicolet Nexus 470) having 10 micron viewing area with single bounce attenuated reflectance device (OMNI Sampler™ with Ge crystal). FTIR of pure chitosan, pure PEO and chitosan-PEO core sheath nanofibers (after washing off PEO) was performed.

5.3.3.3. Scanning and Transmission electron microscopy

To determine the surface morphology of nanofibers obtained from co-axial electrospinning, scanning electron microscopy (SEM) was performed using JEOL JSM-6400 FE with Energy Dispersive X-ray Spectroscopy (EDS) operating at 5 kV. Co-axial nanofibers samples were collected on aluminum foil and were sputter coated by a K-550X sputter coater with Au/Pd having thickness ~ 100 A° to reduce charging.

Transmission electron scanning was performed using FEI/Philips EM 208S operating at 80 kV. The electrospun nanofibers were directly deposited on Copper grids coated with a layer of formvar and carbon film.

5.3.3.4 Mechanical properties

Tensile test were performed using MTS tensile tester for measuring tensile properties of electrospun web. ASTM D882 method of testing was used for the nonwoven electrospun chitosan-PEO (core-sheath) mats. The gauge length of the mats was 3 cm and average thickness was 0.12 mm. Measurements were done at 70° F, 65 % RH and at a strain rate of 5 mm/min. Void volume fraction was calculated using Image J analyzer. SEM images were scanned through Image J, nanofibrous layers were differentiated through a grey scale and area (proportional to volume) of one layer of nanofibers was then calculated.

5.3.3.5 Electrical properties of chitosan-PEO core-sheath and chitosan nanofibers

Electrical measurements utilized planar interdigitated electrodes on glass to measure these highly porous mats of nanofibers, as well as cast films for comparison. This technique allows estimated conductivity to be obtained for very thin (1-10 μm) porous samples where placing electrodes above and below (sandwich-configuration) the sample would lead to pin holes and poorly-defined geometry. Details can be found in a previous publication.[16] In short, the interdigitated electrodes were fabricated from conventional lift-off uv-lithography with a digit spacing of 10 μm, digit length 1 mm, and with each electrode consisting of 50 finger pairs. Mats or films were electrospun or cast onto the pre-prepared electrodes, allowing application of an electric field generally parallel to the substrate. A sensitive Keithley (6430 subfemtoamp) source-measurement unit was used to obtain current-voltage characteristics which were analyzed to obtain electrical conductance. It is well-known that interdigitated electrodes generate significant fringe fields that penetrate above and below the electrode plane, with the depth of penetration proportional to the finger spacing. Based on the calculated field patterns of our interdigitated electrode configuration, values for estimated conductivity were calculated.[61] In particular, assuming a large number of finger pairs and negligible finger thickness compared to other electrode and sample dimensions, an estimate of the electric field versus depth was obtained. To summarize this procedure, for a linear current-voltage response, measured current is proportional to the integrated area under the electric field versus distance curve. Equivalently, a constant electric field can be

assumed with an effective depth of penetration which is roughly equal to the finger spacing, for equal finger width and spacing.

For these experiments, samples in vacuum (~ 1e-7 torr), at ambient conditions, and after one hour soaks in de-ionized water were measured. Samples were either submerged in water or exposed by repeated water drops placed on the surface. Electrospun mats were fabricated as described in Section 2.2 with the electrode placed on the collector plate. Mats with a thickness of ~30-50 μm or ~120-150 μm were measured. Mat height was measured with a micrometer for thicker samples and then extrapolated down for thinner samples assuming that the rate of deposition was constant throughout the spin. Films were cast by placing a drop onto the electrode which spread and dried to a uniform film. In addition, free-standing films (first cast, and then peeled from the surface) were also measured, either by fabrication of contacts with silver epoxy or by placing swollen films onto interdigitated electrodes

3. Results and Discussion

Conductivity measurements showed that as the concentration of Chitosan increased, solution conductivity also increased. Results of the conductivity are shown in Table 1.

Table 1: Solution Properties of Chitosan dissolved in 90 % (w/w) AcOH samples

S. No.	Chitosan Wt %	Conductivity mS/cm
1	1	1.80
2	2	3.31
3	3	4.42
4	4	4.96
5	5	5.77
6	6	6.33
7	7	6.50

Zero shear rate viscosity (η_0) versus concentration is plotted in Figure 2. The η_0 of 3 wt % chitosan (77 cP) and 4 wt % PEO (72 cP) are nearly equivalent. 4 wt % PEO is easily electrospun into defect free nanonfibers, therefore this concentration was used for all experiments. Since the viscosities of these two solutions are similar, the amount of shear stress generated at the tip of the capillary in 4 wt % PEO and 3 wt % chitosan are closely matched. In fact, coaxial nanofibers were produced only with this set of concentrations (3 wt % chitosan/4 wt % PEO), with comparable values of η_0.

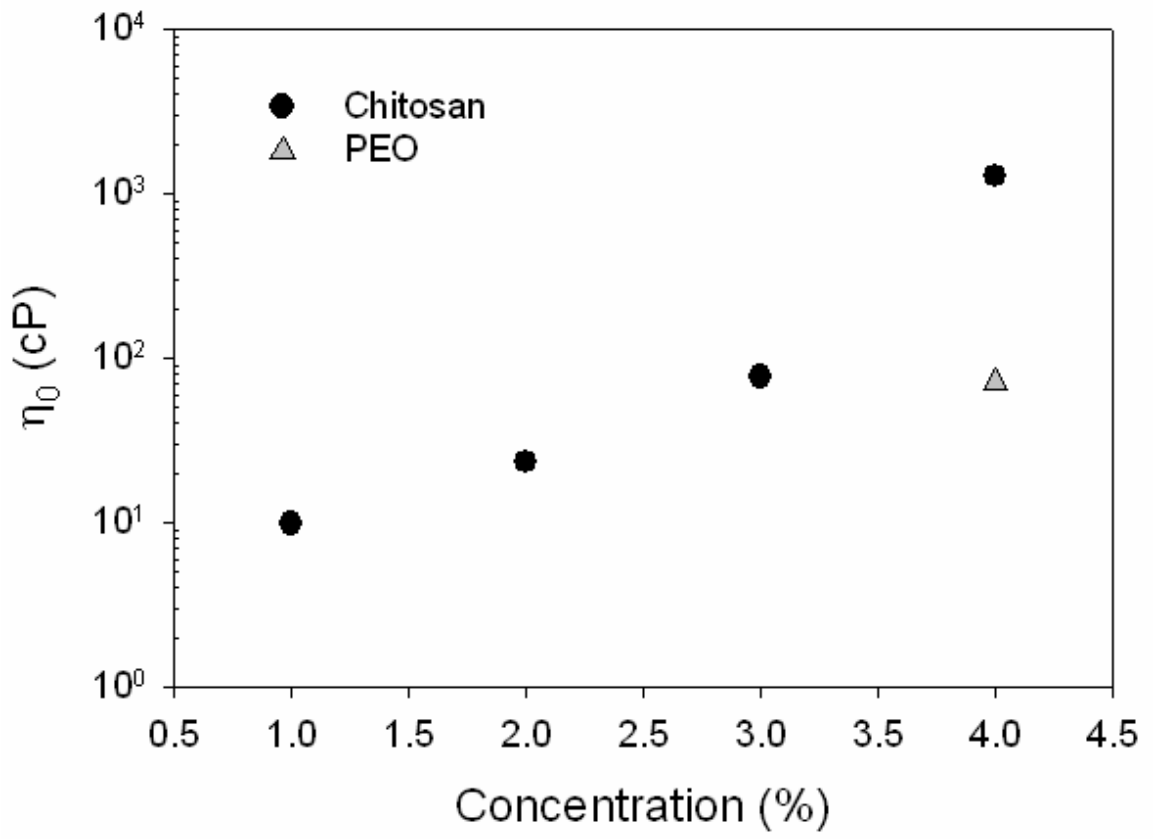

Figure. 2: The concentration dependence of the zero shear rate viscosity (η_0) for chitosan and PEO. The black circles indicate η_0 for varying concentrations of chitosan (1 – 4 wt %) and the gray triangle indicates η_0 for 4 wt % PEO.

TEM investigations shows formation of core-sheath structure and stark contrast is observed between core and sheath nanofiber. Different concentrations of chitosan were utilized (1-7 wt %) but core-sheath morphology was observed with only 3 wt % chitosan solution (as core) together with 4 wt % PEO solution (as sheath). It can be seen that the diameter of the sheath nanofibers obtained is around 250 nm and the diameter of the core nanofiber is around 100 nm. It should be stressed that chitosan is not able to spin by itself

as a monocomponent filament and hence the PEO sheath layer is need to act as carrier for formation of chitosan fibers. (Fig. 3)

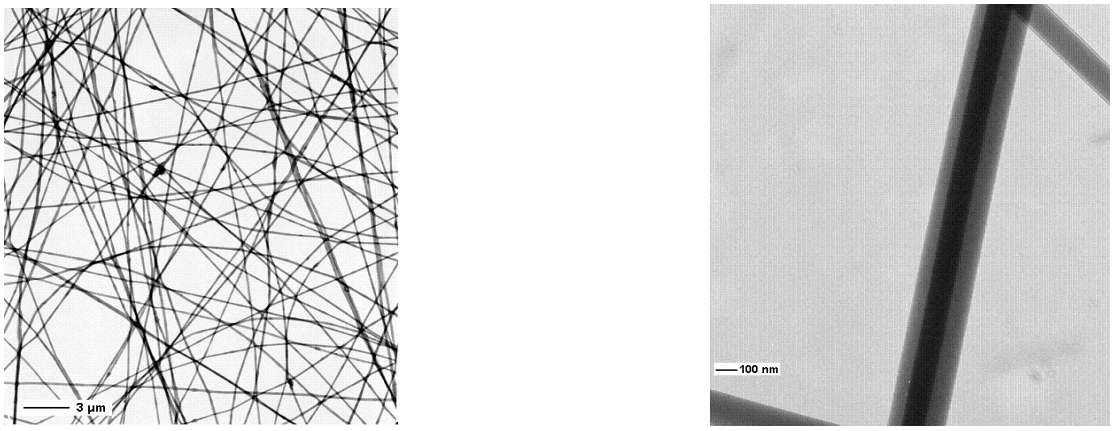

Figure 3: TEM images of coaxially electrospun Chitosan (3 wt %)-PEO (4 wt %) core-sheath fibers before washing out PEO

FTIR results (Fig. 4) confirmed peaks corresponding to chitosan and PEO in the core-sheath assembly. In order to determine qualitatively presence of chitosan as core and PEO as sheath, FTIR was performed before and after the nanofibrous mats were subjected to di-ionized water for 24 hrs. After washing, peaks corresponding to PEO were subdued. We hypothesize that some PEO was still present in the interstitial spaces which was unable to leach out in de-ionized water.

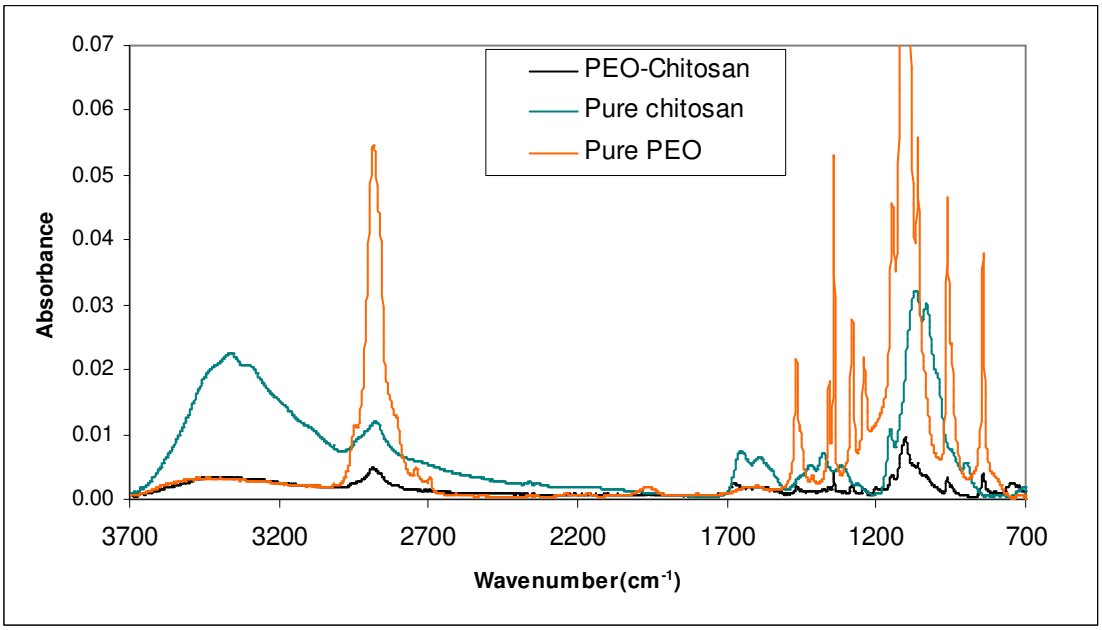

Figure 4: FTIR of electrospun PEO-Chitosan nanofibers (after washing off PEO), PEO and Chitosan

SEM images were taken after the mats were treated with water and they show that the structure and integrity of nanofibers were still maintained. It validates our hypothesis that PEO was washed off from the surface of nanofibers and chitosan insoluble in water remained. Washed nanofibers (essentially chitosan) appeared to be flattened, and bundled together, we hypothesize that this is due to formation of hydrogen bonds with water molecules and as water is evaporated the nanofibers come and bundle together. (Fig. 4)

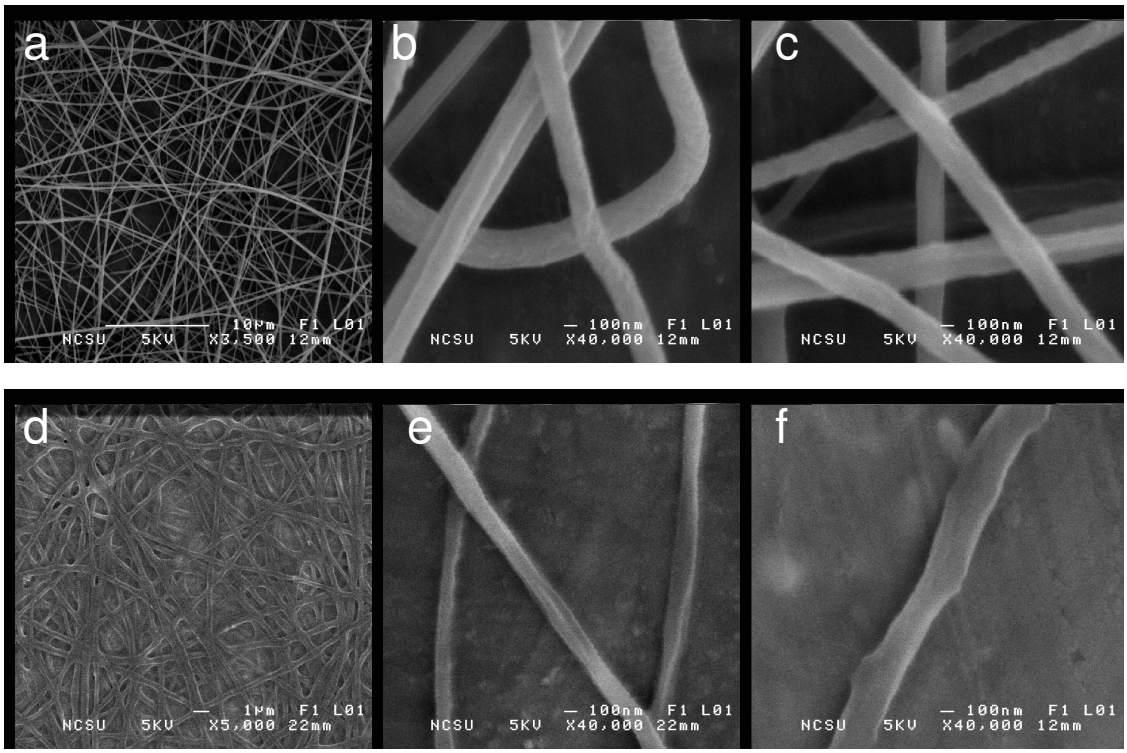

Figure 5. (a-g) SEM images of electrospun chitosan-PEO core-sheath nanofibers. (a-c) samples before H_2O treatment. (d-f) samples after H_2O treatment.

To evaluate the changes mechanical properties of nanofibrous mats due to incorporation of core fluid, five core-sheath (3 wt % Chitosan and 4 wt % PEO) electrospun specimens having identical dimensions were subjected to tensile testing. Void volume fraction obtained from SEM images using Image J analyzer showed about 84 % of total space were voids in one layer of core-sheath nanofibrous mats. If compared from our previous findings,[16] it is evident that with introduction of Chitosan as core fluid, the modulus and tenacity decreases. The decrease in tenacity and modulus could be attributed to high void volume fraction and also due to mismatch in surface energies of the two different polymers. (Table 2)

Table 2: Mechanical Properties of Core-sheath nanofibers before washing off PEO

Chitosan Sample	Tenacity (kgf/mm^2)	Elongation at break (%)	Modulus (kgf/mm^2)
1	0.08	1.7	2.66
2	0.06	1.6	2.24
3	0.07	1.9	2.38
4	0.05	1.1	2.09
5	0.07	1.1	2.67

In addition to the specific morphology of an artificial tissue scaffold, its physical properties, such as degree of hydrophilicity, surface charge, mechanical modulus, and electrical conductivity are likely of importance in allowing natural cell growth and differentiation.[62-64] Furthermore, previous workers have utilized electrically conductive scaffolds to actively stimulate cell proliferation in vitro.[65-66] Natural biopolymers (including collagen and other components of the mammalian extracellular matrix) do have innate conductivity, usually due to ionic motion and with a strong dependence on water concentration.[67] Likewise chitosan is a solid electrolyte which conducts ions when hydrated.[68] Previous studies determined that dry chitosan films measured at ambient conditions (with molecular weights 3e5- 8e5 gm/mol at 70-95% de-acetylation) have conductivity in the range 1e-11 - 1e-9 S/cm.[69] The value rises to 1e-5-1e-4 after exposure to water for one hour or more. A mechanism whereby water protonates amine groups in the backbone forming mobile hydroxyl ions ($H_2O + NH_2 \rightarrow NH_3^+ + OH^-$) has been proposed. Lower molecular weight chitosan showed smaller gains in conductivity with

σ_{max} = 1e-5 S/cm after water exposure, presumably because of increased crystallinity. Here our molecular weight is slightly lower at 1.48e5 gm/mol. In a series of papers, Wan explored a variety of schemes to further increase conductivity above the 1e-4 S/cm value, including crosslinking[70] and chemical modification[71-72] to minimize crystallization. These attempts raised the maximum conductivity by about an order of magnitude. The authors concluded that crystallinity and the related ability of the film to swell were the limiting factors to achieving increased conductivity. As both crystallinity and swelling index may vary for electrospun mats versus drop-cast films, it is valuable to compare the ionic conductivity for chitosan scaffolds with comparable films. Thus electrical conductivity measurements serve three purposes here: 1) to confirm the core-sheath geometry of the PEO-chitosan fibers and the subsequent composition of the (washed) chitoson nanofiber mat; 2) to explore the effects of electrospinning including differences in morphology, swelling index, and crystallinity on chitosan conductivity; and 3) to determine the in-situ conductivity of a chitosan tissue scaffold in a biologically-relevant environment (saline) with an eye to employing such scaffolds for electrical stimulation in tissue engineering.

As discussed in the experimental section, samples consisted of electrospun mats of various thickness directly deposited onto interdigitated electrodes. Drop-cast films of 3 wt% chitosan in 90% acetic acid were utilized as controls. Each electrode was measured before mat or film deposition, with this measured conductance, ~ 1e-14 S in vacuum or ~1e-13 S at ambient, setting the measurement limit of our system. Mats of PEO-chitosan nanofibers, with one exception, perhaps due to incomplete coating with PEO, showed no

conductance, that is a current-voltage characteristic indistinguishable from the un-coated electrode. This result is consistent with the core-sheath picture where the highly insulating PEO completely encapulsates the chitosan core.

After washing with de-ionized water for 24 hours, the chitoson mats were again measured under vacuum and displayed an estimated conductivity of 10^{-12} - 10^{-11} S/cm. The same range of values was observed for drop-cast films and is consistent with previous reports.[73] Removing the samples from vacuum and measuring under ambient conditions resulted in an increase of conductivity to ~10^{-9}, again with mats and films showing similar values. These results are consistent with the values of 1e-9-1e-10 S/cm reported by Wan for dry samples at ambient conditions.[69] For ambient measurements, some current-voltage characteristics displayed a dramatic current increase when voltage was first applied which then decreased to a steady-state value (about 1/2 - 1/3 the initial current) over many minutes, akin to a charging peak in a cyclic voltammogram. Such behavior is often associated with diffusion-limited ionic conduction.[74-76]Because of this effect, voltage was first swept up to its maximum value (over about an hour) and then the quasi steady-state current-voltage characteristic was measured as a function of decreasing voltage. Thicker, free-standing films with silver epoxy electrodes spaced by ~ 1 cm, displayed linear current-voltage characteristics at ambient conditions with conductance values of 10^{-6} S/cm, which is consistent with the interdigitated film values, given the unknown field pattern for the silver epoxy electrodes.

Whereas measurements in vacuum and at ambient conditions were highly reproducible, upon soaking samples in water, a variety of results were obtained. In particular, mats on interdigitated electrodes decreased in conductance when submerged in water, indicating a loss of material. Furthermore, films cast onto a glass slide or interdigitated electrodes, did not exhibit noticeable swelling and showed only moderate gains in conductivity (increasing from ~10^{-9} to 10^{-7} S/cm). In contrast, free standing films, which were peeled from a glass coverslide, displayed a dramatic swelling behavior, transforming from a light-yellow film to a clear gel. When such a swollen film was subsequently placed onto electrodes and measured, it showed a value of 10^{-4} S/cm, consistent with previous reports in the literature. Free-standing films with silver epoxy contacts showed a similar value (1e-5-1e-4 S/cm), when the increased thickness of the films was taken into account. However, the geometry of the electrodes needs to be confirmed in this case. Reproduction of these result and similar experiments with pre-swollen mats are underway.

5.5. Conclusions

In the present work, we have demonstrated that chitosan fibers can be electrospun in a core-sheath configuration with an easily spinnable polymer (such as PEO) in the sheath layer. Fourier transform infrared spectroscopy shows that PEO (outer layer) is removed by washing the core-sheath nanofibers with water. Solution conductivity measurements showed that as the concentration of chitosan increases, conductivity also increases. SEM and TEM investigations confirm core sheath morphology of nanofibers. Tensile tests

show that as chitosan is inserted as core, a decline in mechanical properties was observed as compared to pure PEO nanofibers.

The potential of such nanofibers could be immense in biomedical field involving wound care, tissue engineering to name a few. Cheap and known for its anti-bacterial properties, chitosan definitely is a promising candidate for electrospinning when used in conjunction with another bio-compatible polymer.

5.6. Acknowledgements:

We gratefully acknowledge Dr. Michael Dykstra and Abbey Wood for their efforts in performing TEM. We also thank Dr. Dale Batchelor for helping us with SEM.

5.7. References

1. Reneker, D.H. Chun, I. *Nanotechnology* 1996, 7, 216
2. Kenawy, E.R., Bowlin, G.L., Mansfield, K., Layman, J., Simpson, D.G., Sanders, E.H., Wnek, G.E., *J. Controlled Release* 2002, 81, 57
3. Li, D., Wang, Y., Xia, Y., *Nano. Lett*. 2003, 3 (8), 1167
4. Theron, A., Zussman E., Yarin, A.L., *Nanotechnology* 2001, 12, 384
5. Huang, Z.M., Zhang, Y.Z., Kotaki, M., Ramakrishna, S., *Compos. Sci. Technol*. 2003, 63, 2223
6. Chen, J., Karageorgiou, V., Altman, G.H., Kaplan, D.L., *Biomaterials* 2004, 25 1039
7. MacDiarmid, A.G., Jones, W.E., Norris, I.D., Gao, J., Johnson, A.T., Pinto, N.J., Han, B., Ko, F.K., Okuzaki, H., Llaguno, M., *Synth. Met.* 2001, 119, 27
8. Kim, C., Yang, K.S., *App.l Phys. Lett*. 2003, 83, 1216
9. Drew, C., Liu, X., Zeigler, D., Wang, X., Bruno, F.F., Whitten, J., Samuelson, L.A., Kumar, J., *Nano. Lett.* 2003, 3 (2), 143
10. Khil, M.S., Cha, D.I., Kim H.Y., Kim, I.S., Bhattrai, N., J. *Biomed. Mater. Res. Part B: Appl. Biomater.* 2003, 67B, 675
11. Tsai, P.P., Schreuder-Gibson, H., Gibson, P., *J. Electrostat.* 2002, 54, 333
12. Shao, C., Kim, H.Y., Gong, J., Ding, B., Lee, D.R., Park, S.J., *Mater. Lett*. 2003, 57, 1579
13. Formhals, A., US Patent 1, 975,504, 1934
14. Reznik, S.N., Yarin A.L., Theron, A, Zussman, E.,*J. Fluid Mech*., 2004, 516, 349

15. Hohman, M.M., Shin, Y.M., Rutledge, G.C., Brenner, M.P., *Phys. Fluids*, 2001, 13, 2201

16. McCullen, S.D., Stevens, D.R., Roberts, W.A., Ojha, S.S., Clarke, L.I., Gorga, R.E., Macromolecules, 2007, 40 (4), 997

17. Fong, H., Chun, I., Reneker, D.I., *Polymer*, 1999, 40, 4585

18. Lee, K.H., Kim, H.Y., La, Y.M., Lee, D.R., Sung, N.H., *J. Poly. Sci. Part B: Poly. Phys.* 2002, 40, 2259

19. Liu, H., Hseih, Y.L., *J. Poly. Sci. Part B: Poly. Phys*. 2002, 40, 2119

20. Demir, M.M., Yilgor, I., Yilgor, E., Erman, B., *Polymer*, 2002, 43, 3303

21. C. Li, C. Vepari, H.-J. Jin, H. J. Kimand D. Kaplan, *Biomaterials*, **27**, 3115-3124 (2006)

22. Bhattarai S.R., Bhattarai, N., Vishwanathamurthy, P., Yi, H.K., Hwang, P.H., Kim, H.Y., J. Biomed. Res. Part A, 2006, 247

23. He, W., Ma, Z-W., Yong, T., Teo W.E., Ramakrishna, S., Biomaterials 2005, 26, 7606

24. Xin, X., Hussain, M., Mao, J.J., Biomaterials, 2007, 28, 316

25. Zhang, Y., Huang, Z.M., Xu, X., Lim, C.T., Ramakrishna, S., *Chem Mater*., 2004, 16, 3406

26. Jang, J., Lim, B., Lee, J., hyeon, T., *Chem Commun.,* 2001, 1, 83

27. Morales, A.M., Leiber, C.M., *Science*, 1998, 279, 208

28. Bognitzki, M., Hou, H., Ishaque, M., Frese, T., Hellwig, M., Schwarte, C., Schaper, A., Wendorff, J.H., Greiner, W., *Adv. Mater.* 2000, 12, 9, 637

29. Xie, Y., Qiao, Z.P., Chen, M., Liu, X.M., Qian, Y.T., *Adv.Mater.* 1999, 11, 1512

30. Yu, J.H., Fridrikh, S.V., Rutledge, G.C., *Adv. Mater.,* 2004, 16, (17), 1562

31. Sun, Z., Zussman, E., Yarin, A., Wendorff, J.H., Greiner, A., *Adv Mater*., 2003, 15, 22, 1929

32. Li, D., Xia, Y., Nano. Lett., 2004, 4 (5), 933

33. Gupta, P., Wilkes, G.L., *Polyme*r, 2003, 44,6353

34. Loscertales, I.G., Barrero, A., Guerrero, I., Cortijo, R., Marquez, R., Ganan-Calvo, A.M., *Science*, 2002, 295, 1695

35. Zhang, Y.Z., Wang, X., Feng, Y., Li, J., Lim, C.T., Ramakrishna, S., *Biomacromolecules*, 2006, 7, 1049

36. Song, T., Zhang, Y., Zhou, T., Lim, C.T., Ramakrishna, S., Liu, B., *Chem. Phys. Lett.*, 2005, 415, 317

37. Wang, M., Yu, J.H., Kaplan, D.L., Rutledge, G.C., *Macromolecules*, 2006, 39, 1102

38. Li, D., Babel, A., Jenekhe, S.A., Xia, Y., Adv. Mater. 2004, 16 (22), 2062

39. Suh, J.KF., Matthew, H.W.T., *Biomaterials*, 2000, 21, 2589

40. Borchard, G., *Adv. Drug. Deliv. Rev.,* 2001, 52, 145

41. Tomihata, K., Ikada, Y., *Biomaterials*, 1997, 18, 567

42. Kang, D.W., Choi, H.R., Keon, D.K., *J. Appl. Poly. Sci*. 1999, 73, 469

43. Peniche, C., Arguelles-Monal, W., Devidenko, N., Sastre, R., Gallardo, A., San Roman, J., *Biomaterials*, 1999, 20, 1869

44. Lee, W.F., Chen, Y.J., *J. Appl. Poly. Sci.* 2001, 82, 2487

45. Percot, A., Viton, C., Domard, A., *Biomacromolecules*, 2003, 4, 12

46. Lim, S.H., Hudson, S.M., *J. Macromol. Sci.- Polym. Rev.,* 2003, C43, 223

47. Li, L., Hsieh, Y.L., *Carbohydrate Research*, 2006, 341, 374

48. Amaike, M, Senoo, Y and Yaamoto, H., *Macromol. Rapid Commun.* 1998, 19, 287

49. Bhattarai, N., Edmondson, D., Omid V., Matsen, F.A., Zhang, M., *Biomaterials*, 2005, 26, 6176

50. Duan, B., Dong C., Yuan, X., Yao, K., *J. Biomater. Sci. Polymer Ed*., 2004, 15 (6), 797

51. Ohkawa, K., Cha, D.I., Kim, H., Nishida, A., Yamamoto, H., *Macromol. Rapid Commun*., 2004, 25, 1600

52. Chen, C.Y., Wang, J.W., Hon, M.S., *Macromol. Mater. Eng*., 2006, 291, 123

53. Min, B.M., Lee, S.W., Lim, J.N., You, Y., Lee, T.S., Kang, P.H., Park, W.H., *Polymer*, 2004, 45, 7137

54. Minami, S., Okamoto, Y., Matsuhashi, A., Application of chitin and chitosan in large animal practice. In: Brine CJ, Sandford PA, Zikakis JP, editors. Advances in chitin and chitosan. New York: Elsevier, 1992, 61

55. Minami, S., Okamoto, Y., Tanioka, S., Effects of chitosan on wound healing. In: Yalpani M, editor. Carbohydrates and carbohydrate polymers. Mount Prospect. IL, USA: ATL Press, 1992, 142

56. Barbul, A., Regan, M.C., *Otolaryngol Clin North Am* 1995, 28, 955

57. Badgett, A., Bonner, J.C., Brody, A.R., *Lipid Mediat Cell Signal* 1996, 13, 89

58. Subramanian, A., Vu, D., Larsen, G.F., Lin, H-Y., J. *Biomater. Sci. Poly. Edn*., 2005, 16 (7), 861

59. Bhattarai, N., Edmondson, D., Veiseh, O., Matesn, F.A., Zhang, M., *Biomaterials*, 2005, 26, 6176

60. Van Gerwen, P., Laureyn, W., Laureys, W., Huyberechts, G., Op De Beeck, M., Baert, K, Suls, J., Sansen, W., Jacobs, P., Hermans, L., Mertens, R., *Sensors and Actuators B,* 1998, 49, 73

61. den Otter, M., *Sensors and Actuators A,* 2002, 96, 140

62. Taiji Adachi, Yuki Osako, Mototsugu Tanaka, Masaki Hojo, Scott J. Hollister, *Biomaterials*, 2006, 27, 3964

63. Krishna Prasad Chennazhy, Lissy K. Kishnan, *Biomaterials*, 2005, 26, 5658

64. Lorenzo Moroni, Ruud Licht, Jan de Boer, Joost R. de Wijn, Clemens A. van Blitterswijk, *Biomaterials*, 2006, 27, 4991

65. Arundhati Kotwal, Christine E. Schmidt, *Biomaterials,* 2001, 22, 1055

66. P. R. Supronowicz, P. M. Ajayan, K. R. Ullmann, B. P. Arulanandam, D. W. Metzger, R. Bizios, *J Biomed Mater Res* 2002, 59, 499

67. W.Y. Gu, M.A. Jutiz, *Journal of Biomedical Engineering*, 2002, 124, 790

68. Ernesto López-Chávez, José Manuel Martínez-Magadán, Raúl Oviedo-Roa, Javier Guzmán, Joel Ramírez-Salgado, Jesús Marín-Cruz, *Polymer*, 2005, 46, 7519

69. Ying Wan, Katherine A.M. Creber, Brant Peppley, V. Tam Bui, *Polymer*, 2003, 44, 1057

70. Ying Wan, Katherine A.M. Creber, Brant Peppley, V. Tam Bui, *Journal of Applied Polymer Science,* 2003, 89, 306

71. Ying Wan, Katherine A.M. Creber, Brant Peppley, V. Tam Bui, *Macromolecular Chemistry and Physics,* 2003, 204, 850

72. Ying Wan, Katherine A.M. Creber, Brant Peppley, V. Tam Bui, *Journal of Polymer Science: Part B, Polymer Physics*, 2004, 42, 1379 (2004).

73. Tkaczyk, S.W., Swiatek, J., Mucha, M., *IEEE Transactions on Dielectrics and Electrical Insulation,* 2001, 8 (3), 411

74. Casalbore-Miceli, G., Campos, M., Beggiato, G., *Solid State Ionics* 1995, 80, 239

75. Sodolski, H., Kozlowski, M., *Solid State Ionics* 1999, 119, 109

76. Celzard, A., McRae, E., Furdin, G., Marêché, J.F., *Journal of Physics: Condensed Matter,* 1997, 9, 2225

Chapter 6

Dependence of percolation threshold and mechanical properties on morphology of nanofibers

*Satyajeet S Ojha[1], Derrick R Stevens[2], Torissa Hoffman[2], Laura Clarke[2] and Russell E. Gorga[1]**

[1]Department of Textile Engineering, Chemistry and Science, [2]Department of Physics, North Carolina State University

6.1. Abstract:

The present work focuses on fabrication of nanocomposite fibers having novel core-sheath morphologies. Multi-walled carbon nanotubes (MWCNTs), due to their superior mechanical and electrical properties have been utilized to construct such nanocomposites. Sub-micron diameter sized nanofibers (200-300 nm) encapsulating MWCNTs were produced with remarkable increase in conductance. MWCNT concentration to reach the percolation threshold was less than half in the case of core-sheath (having MWCNTs in sheath layer) nanofibers as compared to MWCNTs loaded in a single layer nanofiber. Mechanical testing demonstrated that tensile strength did not vary but Young's modulus increased appreciably. It also showed that a concentration of 0.25 weight percent (wt %) of MWCNTs was optimum in case of core-sheath nanofibers and after that a decrease in modulus as well tensile strength was seen.

Keywords: electrospinning, nanotubes/polymer composites, conductivity, percolation.

6.2. Introduction

Electrospinning is a simple technique employed to generate fibers having diameter at sub-micrometer range. Electrostatic forces instead on mechanical forces are utilized in this procedure[1]. In this process a pendant polymer solution droplet, typically conical in shape is charged either positively or negatively until the static charge repulsion overcome surface tension resulting in a highly extensional flow. As a consequence, ultrahigh drawing of fibers takes place and exceedingly fine fibers are produced[2-3]. These nanofibers have very high surface to volume ratio which makes them ideal candidates drug delivery[4], tissue engineering[5], conductive nanowires[6], super-capacitors[7], nanosensors[8], wound dressings[9] and filtration membranes.[10-11]

Discovery of Carbon nanotubes (CNTs) has given a great thrust in nanoscience and nanotechnology. These nanotubes are essentially seamless rolled graphitic sheets. Both single (SWCNTs) and multi-walled (MWCNTs) have superior structural, mechanical, electrical, chemical and thermal properties. Carbon nanotubes have very high aspect ratio (> 1000) which makes them ideal candidates for composites.[12-16] Due to such impressive properties a lot of interest has been received in fabrication of nanocomposite fibers reinforced with CNTs.[2, 17-22] Owing to very high surface area these nanotubes tend to aggregate as a result of van der Waals interaction and form bundles in order to lower their surface energy. To utilize full potential in terms of mechanical and electrical properties, proper dispersion of these moieties is of utmost importance. Predominantly, four methods have been employed to achieve dispersion they are: mechanical methods,[23-24]

functionalizing the SWNTs,[25-30] using surfactants[31]and non-covalent modification by using small molecules and polymer dispersants.[32-39]

Separation of individual nanotubes is a challenging problem and has attracted a lot of research. Vigolo et al. have demonstrated dispersion on CNTs using Sodium dodecyl sulfate (SDS). Subsequently, they have also reported spinning of CNTs from an aqueous dispersion of SDS.[40-42] Similarly, O'Connell and coworkers have utilized an amphiphilic polymer, poly (vinyl pyrrolidone) for dispersion of CNTs.[43] In other analysis, Islam et al. have made a nice comparison of different surfactants including commercial available Triton X-100 for high weight fraction solublization of SWNTs.[31] Gum Arabic a naturally occurring polysaccharide have been used as surfactant to disperse CNTs and achieve high level of nanotube orientation[44-45]

Electrospinning is an efficient way to fabricate nanocomposite fibers doped with CNTs. Recent works have shown electrospinning as a feasible technique to incorporate CNTs in nanofibers.[46-48]Mechanical and electrical properties of nanofibers exhibit improvement upon addition of CNTs as fillers in polymeric nanofibers.[16]

In electrospinning, due to high shear at the tip of the needle nanotubes, which were previously dispersed, get aligned. Adequate dispersion and alignment of fillers such as carbon nanotubes facilitates transformation of insulating properties of matrix component into conductive as a result of development of networks of filler material. The critical point where this transformation takes place is called as percolation threshold. Below

percolation threshold, conductance is only through insulator matrix. Percolation threshold depends upon volume fraction as well as conductivity of fillers.

Nanofibers having core-sheath structure is a subject of interest in current research. These core-sheath nanofibers due to their characteristic configuration could be potentially applied in a variety of fields such as sustained delivery of drugs, preservation of biological agent from externally aggressive environment.[49] Many strategies have been developed to fabricate nano- and mesocables using TUFT (tube by fiber template) process,[50] growth of semiconductor nanowires inside polymer tubules incorporating electrospinning.[51]

Fabrication of coaxial or core-sheath nanofibers is realized by injecting polymer solutions or melts through two annular orifices into a region of uniform electric field. Such a technique to produce coaxial nanofibers is advantageous when one polymer component is incapable of forming nanofibers due to its inherent fluid characteristics. Morphology of these nanofibers depends on a lot of factors such as viscosity, shear stresses, bending stability and Maxwell stresses. These properties should be almost same or in vicinity of each other for the two polymers used in coaxial electrospinning.

Several efforts have been made in order to comprehend evolution of single jet of various polymers. Hohman and Feng have put forward a quasi-uni-directional model to compute induced electric field by charged jets.[52-53] Higuera in his recent work has attempted to investigate in great detail properties and conditions of existence of coaxial jets extending

the quasi-uni-directional model, considering flow rate, surface tension and viscosity of two fluids.[54-55]

In this work we attempt to produce coaxial nanofibers having pure PEO as core and PEO doped with different concentration (in weight %) of MWCNTs as sheath. The electrospinning process is very fast so that the two jets of polymers do not mix.[56]Our goal through this work is to characterize percolation behavior of coaxial nanofibers comparing it with single layer nanofibers, to visualize effect of volume constraint on conductance behavior of MWCNTs and consequently change in mechanical properties as a function of MWCNT loading.

6.3. Experimental

6.3.1. Materials

Polyethylene oxide (PEO) of M_w 900,000 was obtained from Scientific Polymer Products. MWNTs supplied by Nano-Lab were produced by plasma enhanced chemical vapour deposition (CVD) using acetylene and ammonia with an iron based catalyst and were grown on mesoporous silica substrate.[57] The diameter and length of these nanotubes was 15 ± 5 nm and 5-20 μm respectively with 95 % purity. MWNT were dispersed in de-ionized water using Ultrasonic model 2000U generator and probe operating at 25 Hz for one hour. Gum Arabic was used at a constant concentration of 3 wt % to aid dispersion in all samples. Concentration of MWNT was varied from 0.1-3.0 wt %. Core fluid (pure

PEO) was stained with bromophenol to obtain a contrast under transmission electron microscopy.

6.3.2. Electrospinning

Electrospinning was performed using two perpendicularly placed programmable syringe pumps (New Era NE 500). The feed rates used for both core and sheath component in coaxial nanofibers were 50 µl/min, to keep equal mass flow rate. The distance between the tip and the grounded electrode was kept constant at 15 cm. Two concentric capillaries were used having diameters 16G and 20G for sheath and core fluid respectively. Fig. 1 shows the design of our electrospinning set-up.

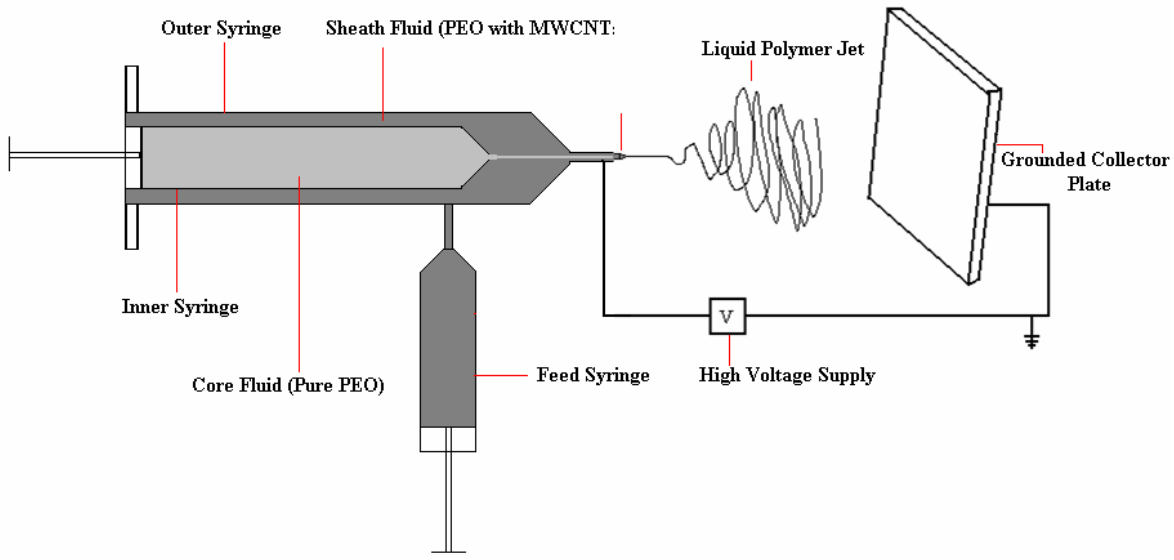

Figure 1. Electrospinning set-up used in core-sheath electrospinning

6.3.3. Characterization

Morphology of nanofibers obtained from co-axial electrospinning was determined through scanning electron microscopy (SEM) using JEOL JSM-6400 FE with Energy Dispersive X-ray Spectroscopy (EDS) operating at 5 kV. Co-axial nanofibers samples were collected on aluminum foil and were sputter coated by a K-550X sputter coater with Au/Pd having thickness ~ 100 A° to reduce charging.

Transmission electron scanning was performed using FEI/Philips EM 208S operating at 80 kV. The electrospun nanofibers were directly deposited on Cu grids coated with a layer of formvar and carbon film.

Electrical measurements were carried out using remote source meter (Keithley, 6430 sub-femtoamp). Using lift-off standard photolithography technique, flat interdigitated electrodes on glass substrate were made followed by thermal evaporations of ~ 150 A° of chromium and ~1150 A° of gold to measure conductance of fibrous mats. Each electrode consisted of 26 finger pairs with 1 mm long, 10 μm wide digits spaced by 10 μm, and two contact pads of ~1 mm^2 each. Each electrode was measured before and after sample deposition, nominally from -10 to 10 V with 0.1 V steps and a 15 s wait after the application of a voltage change. The sample space was evacuated to ~1 x 10^{-7} Torr. Electrospun nanocomposite fibers are highly porous having porosity higher than 60 %. With such a porosity, its difficult to ascertain density of polymer in the nanofibrous mats. To alleviate this problem, conductance instead of conductivity has been reported.

Thickness of the electrospun samples was kept constant by keeping the time and other conditions constant for each of them. As in case of TEM, nanofibers were directly electrospun on these electrodes. Solution conductivity was measured using Orion conductivity/salinity/temperature meter (model # 162). Results of the conductivity are shown in Fig 2.

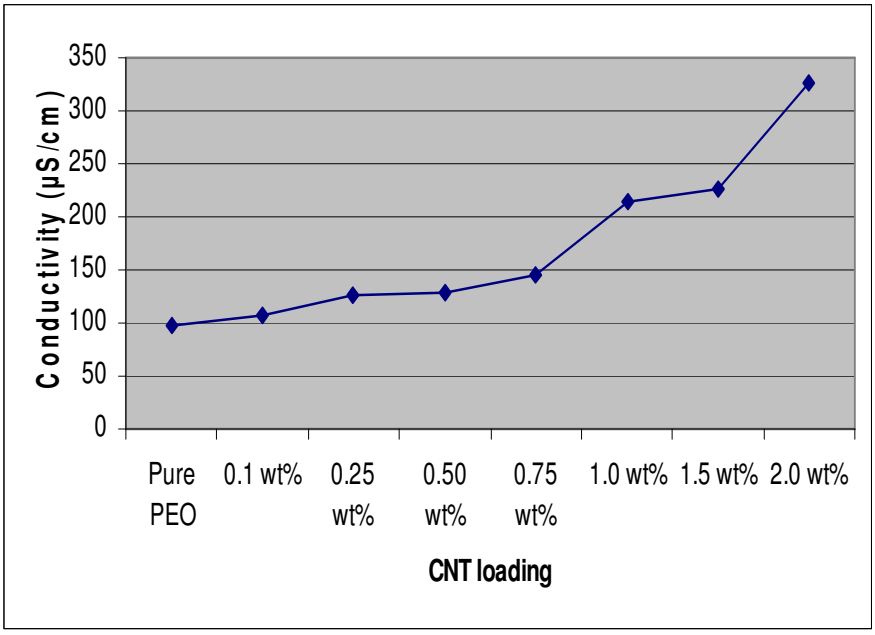

Figure 2. Solution conductivity of polymer solution (PEO) doped with MWCNTs

Void volume fraction or porosity of nanofibrous mats was calculated using Image J analyzer. SEM images were scanned through Image J and layers of nanofibers were differentiated through a grey scale. The length scale of diameter of these nanofibers in one layer forming the width is insignificant as compared to the length of the nanofibers, making them essentially two dimensional. Hence, the void area in one single layer could be approximated as void volume fraction.

Tensile tests were performed using an Instron model 5544 using the Bluehill version 1.00 software. Samples were prepared according to ASTM standard D4762-04. The gauge length of the mats was 3 cm and average thickness was 0.12-0.14 mm. Measurements were done at 70° F, 65 % RH and at a strain rate of 5 mm/min.

6.4. Results and Discussion

Scanning electron micrographs show uniform nanofibers with diameter around 200 nm. Morphology of core-sheath nanofibers appears to be no different than single layer nanofibers from same polymer (PEO). Fig. 3 shows the scanning electron micrographs of single layer as well as coaxial nanofibers.

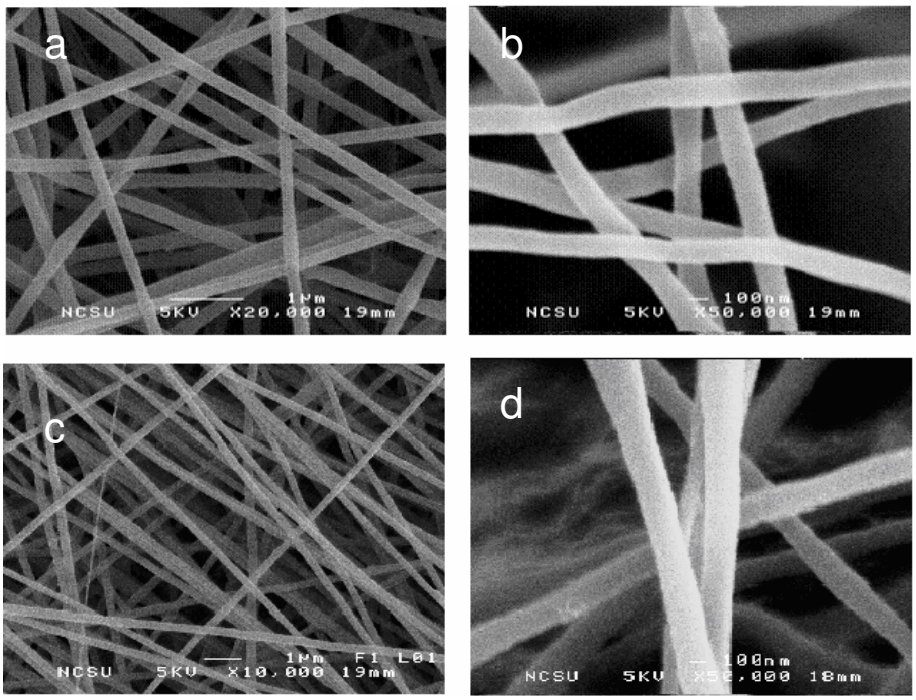

Figure 3. Scanning electron images of single layer nanofibers (a, b) and core-sheath nanofibers (c, d)

In order to investigate and verify the core-sheath morphology of electrospun nanofibers, transmission electron microscopy was utilized. It is evident from Fig 4 that the obtained nanofibers have discernible core of pure polymer (PEO) and sheath of polymer doped with MWCNTs. In our previous work we demonstrated that addition of MWCNTs has minute effect on the rheology of the polymer solution.[16] From the micrographs diameter of the core component was calculated as ~ 40-50 nm.

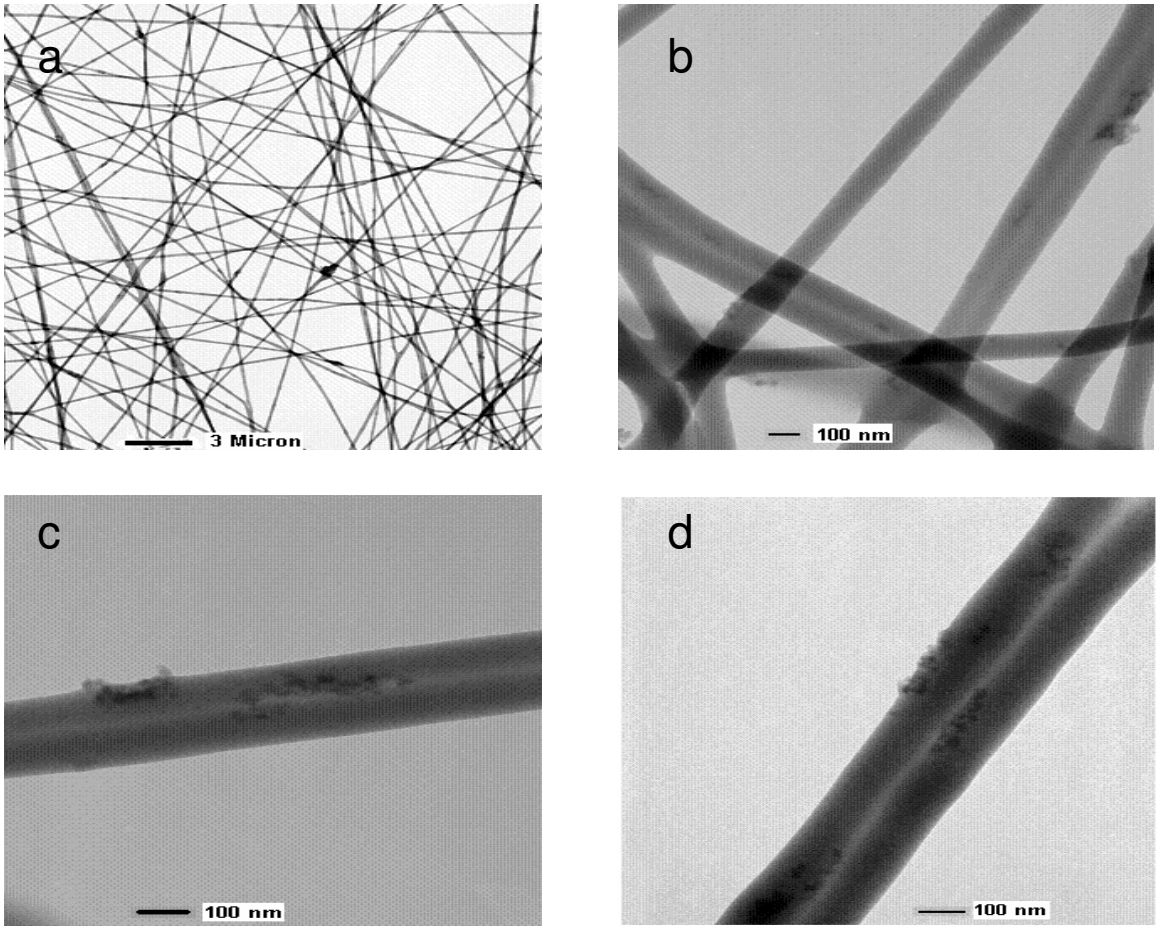

Figure 4. Transmission electron micrographs of PEO (core)/ PEO with MWCNTs (sheath) coaxial nanofibers. (b) 0.05 wt % MWCNTs; (c) 0.25 wt % MWCNTs; (d) 0.50 wt % MWCNTs. Aggregation is observed as the concentration of MWCNTs is increased

In order to determine any changes due in mechanical properties due to insertion of core component and inclusion of MWCNTs, tensile testing was performed. Since the core and sheath material were maintained at similar feed rate, overall concentration of MWCNTs was half of actual concentration in the core component. Tensile testing was performed on three samples having different overall wt % (0.05, 0.25, 0.50) of MWCNTs. At low concentration of nanotubes, good dispersion was achieved but as the concentration of nanotubes increased, tendency to aggregate also increased, as seen in the transmission electron micrographs. These aggregations act as stress concentrations which give rise to low mechanical properties. Results showed that nanofibers having 0.25 wt % nanotubes concentration had appreciable mechanical properties as compared to other samples (Table 1). At 0.5 wt % concentration aggregation of nanotubes was observed.

Table 1. Comparison of mechanical properties of single layer and core-sheath nanofibers

Sample	**MWCNT Concentration (wt %)**	**Effective MWCNT Concentration (wt %)**	**Tensile Strength (MPa)**	**Modulus (MPa)**	**Void Volume Fraction (%)**
Pure PEO (single layer)	0	0	2.49	3.07	75
PEO (single Layer)	3	3	1.26	5.89	75
PEO (core)/PEO w/ MWCNTs (sheath)	0.1	0.05	0.84	19.67	73

PEO (core)/PEO w/ MWCNTs (sheath)	0.50	0.25	1.93	45.49	74
PEO (core)/PEO w/ MWCNTs (sheath)	1.0	0.50	1.30	12.61	76

Mats of the core-sheath nanofibers were spun directly on interdigitated electrodes with multiple weight percentages. From these values a conductance curve was created and fit. As shown in figure 5, it is evident that the percolation threshold for the core-sheath fibers is much lower than for the single component. Fits of the data provide percolation thresholds of 0.45 and 0.013 for the single and bi-component fibers respectively. When explaining this phenomenon many factors must be taken into consideration. There are two mechanisms by which conducting paths may form in the mats. A conducting path may form from connecting multiple fibers to create a single path, or each individual fiber may contain a complete path. The main differences between the single and bi-component fibers are: an available volume reduction, less angular freedom, and a higher concentration of nanotubes close to the outer edge of the nanofiber. The volume reduction and angular distribution are related in that a smaller fiber diameter (or sheath confinement) directly leads to more aligned nanotubes. In addition, with a greater concentration of nanotubes near the fiber surface inter-fiber connections become more probable at lower weight percentages. As to the volume reduction, ignoring it would roughly double the threshold value which is still significantly below that of the single component fiber. It has been shown that an increase in alignment leads to an increase in

the threshold values. While the nanotubes are more aligned in the core-sheath fiber this effect is minimized when looking over the entire mat. The nanotube angular distribution within each fiber is constrained, but the fiber itself may take advantage of the entire space. When looking at the fibers individually the observed thresholds are impossibly low. The minimum number of nanotubes required to complete one path along the length of a fiber leads to a wt% many times larger what is seen. This alone suggests that conductance across the mat is dominated by fiber-fiber connections. With that in mind the greater concentration of nanotubes near the surface in the core-sheath geometry would explain the lower percolation threshold.

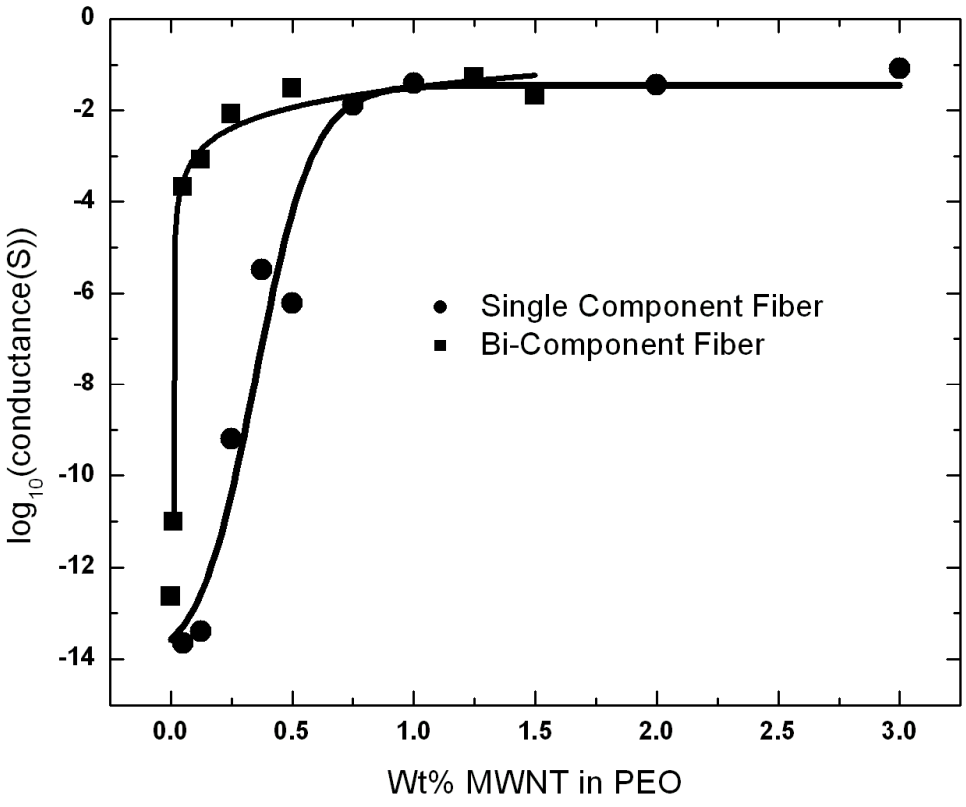

Figure 5: Conductance values for single and bi-component fibers. Wt% values for the bi-component fiber were adjusted to reflect the wt% of the total fiber.

6.5. Conclusion

In the present work, electrospinning has been used as a facile technique to fabricate core-sheath nanofibers with pure PEO as core component and PEO doped with multi-walled carbon nanotubes as sheath component. Scanning electron microscopy has shown that nanofibers formed are similar to those of single layer nanofibers. Core-sheath structure was verified by transmission electron microscopy. Conductivity measurements have shown that percolation threshold is significantly lower for the core sheath morphology as compared to the single component. Decrease in percolation threshold is advantageous from the economic point of view as carbon nanotubes are still expensive and high conductivity has been obtained at relatively lower concentration of nanotubes.

6.6. Acknowledgements

We would like to acknowledge Dr. Dale Batchelor for SEM. We also thank Dr. Michael Dykstra and Abbey Wood for their use of their TEM.

6.7. References

1. Formhals, A., US Patent 1, 975,504, 1934
2. Reneker, D. H.; Chun, I. Nanotechnology **1996**, 7, 216.
3. Bognitzki, M.; Czado, W.; Frese, T.; Schaper, A.; Hellwig, M.; Steinhart,M.; Greiner, A.; Wendroff, J. H. *Adv. Mater.* **2001**, *13*, 70.
4. Kenawy, E.R., Bowlin, G.L., Mansfield, K., Layman, J., Simpson, D.G., Sanders, E.H., Wnek, G.E., *J. Controlled Release* 2002, 81, 57
5. Chen, J., Karageorgiou, V., Altman, G.H., Kaplan, D.L., *Biomaterials* 2004, 25 1039
6. MacDiarmid, A.G., Jones, W.E., Norris, I.D., Gao, J., Johnson, A.T., Pinto, N.J., Han, B., Ko, F.K., Okuzaki, H., Llaguno, M., *Synth. Met.* 2001, 119, 27
7. Kim, C., Yang, K.S., *App.l Phys. Lett*. 2003, 83, 1216
8. Drew, C., Liu, X., Zeigler, D., Wang, X., Bruno, F.F., Whitten, J., Samuelson, L.A., Kumar, J., *Nano. Lett.* 2003, 3 (2), 143
9. Khil, M.S., Cha, D.I., Kim H.Y., Kim, I.S., Bhattrai, N., J. *Biomed. Mater. Res. Part B: Appl. Biomater.* 2003, 67B, 675
10. Tsai, P.P., Schreuder-Gibson, H., Gibson, P., *J. Electrostat.* 2002, 54, 333
11. Shao, C., Kim, H.Y., Gong, J., Ding, B., Lee, D.R., Park, S.J., *Mater. Lett*. 2003, 57, 1579
12. Iijima, S. *Nature* **1991**, *354*, 56.
13. Baughman, R. H.; Zakhidov, A. A.; de Heer, W. A. *Science* **2002**, *297*, 787.
14. Collins, P. G.; Arnold, M. S.; Avouris, Ph. *Science* **2001**, *292*, 706.

15. Yu, M.-F.; Lourie, O.; Dyer, M. J.; Moloni, K.; Kelly, T. F.; Ruoff, R. S. *Science* **2000**, *287*, 637

16. McCullen, S.D., Stevens, D.R., Roberts, W.A., Ojha, S.S., Clarke, L.I., Gorga, R.E., Macromolecules, 2007, 40 (4), 997

17. B. Vigolo, A. Penicaud, C. Coulon, C. Sauder, R. Pailler, C. Journet, P. Bernier, and P. Poulin, Science **290**, 1331 (2000).

18. A. B. Dalton, S. Collins, E. Munoz, J. M. Razal, V. H. Ebron, J. P. Ferraris, J. N. Coleman, B. G. Kim, and R. H. Baughman, Nature (London) **423**, 703 (2003)

19. F. Ko, S. Khan, A. Ali, Y. Gogotsi, N. Naguib, G. Yang, C. Li, H. Shimoda, O. Zhou, M. J. Bronikowski, R. E. Smalley, and P. A. Willis, *Proceedings of the American Institute of Aeronautics and Astronautics*, 2002, p. 1426.

20. F. Ko, Y. Gogotsi, A. Ali, N. Naguib, H. Ye, G. Yang, C. Li, and P. Willis, Adv. Mater. (Weinheim, Ger.) **15**, 1161 (2003).

21. H. Lam, N. Titchenal, N. Naguib, H. Ye, Y. Gogotsi, and F. Ko, Mater. Res. Soc. Symp. Proc. **791**, Q10.5.1 (2003).

22. Y. Dror, W. Salalha, R. L. Khalfin, Y. Cohen, A. L. Yarin, and E. Zussman, Langmuir **19**, 7012 (2003).

23. Park, C.; Ounaies, Z.; Watson, K. A.; Crooks, R. E.; Smith, J. G., Jr.; Lowther, S. E.; Connell, J. W.; Siochi, E. J.; Harrison, J. S.; St. Clair, T. L. *Chem. Phys. Lett.* **2002**, *364*, 303-308.

24. Lin, T.; Bajpai, V.; Ji, T.; Dai, L. *Aust. J. Chem.* **2003**, *56*, 635-651.

25. Chen, J.; Hamon, M. A.; Hu, H.; Chen, Y.; Rao, A. M.; Eklund, P. C.; Haddon, R. C. *Science* **1998**, *282*, 95-99.

26. Niyogi, S.; Hamon, M. A.; Hu, H.; Zhao, B.; Bhowmik, P.; Sen, R.; Itkis, M. E.; Haddon, R. C. *Acc. Chem. Res.* **2002**, *35*, 1105-1113.

27. Aizawa, M.; Shaffer, M. S. P. *Chem. Phys. Lett.* **2003**, *368*, 121- 124.

28. Banerjee, S.; Wong, S. S. *J. Am. Chem. Soc.* **2002**, *124*, 8940-8948.

29. Bahr, J. L.; Tour, J. M. *Chem. Mater.* **2001**, *13*, 3823-3824.

30. Smith, J. G., Jr.; Connell, J. W.; Delozier, D. M.; Lillehei, P. T.; Watson, K. A.; Lin, Y.; Zhou, B.; Sun, Y. P. *Polymer* **2004**, *45*, 825-836.

31. Islam, M. F.; Rojas, E.; Bergey, D. M.; Johnson, A. T.; Yodh, A. G. *Nano Lett.* **2002**, *3*, 269-273.

32. O'Connell, M. J.; Boul, P.; Ericson, L. M.; Huffman, C.; Wang, Y.; Haroz, E.; Kuper, C.; Tour, J.; Ausman, K. D.; Smalley, R. E. *Chem. Phys. Lett.* **2001**, *342*, 265-271.

33. Steuerman, D. W.; Star, A.; Narizzano, R.; Choi, H.; Ries, R. S.; Nicolini, C.; Stoddart, J. F.; Heath, J. R. *J. Phys. Chem. B* **2002**, *106*, 3124-3130.

34. Curran, S.; Ajayan, P. M.; Blau, W. J.; Carroll, D. L.; Coleman, J. N.; Dalton, A. B.; Davey, A. P.; Drury, A.; McCarthy, B.; Maier, S.; Stevens, A. *Ad*V*. Mater.* **1998**, *10*, 1091-1093.

35. Viswanathan, G.; Charapani, N.; Yang, H.; Wei, B.; Chung, H.; Cho, K.; Ryu, C.; Ajayan, P. M. *J. Am. Chem. Soc.* **2003**, *125*, 9528- 9259

36. Curran, S.; Davey, A. P.; Coleman, J. N.; Dalton, A. B.; McCarthy, B.; Maier, S.; Drury, A.; Gray, D.; Brennan, M.; Ryder, K.; La Chapelle, M. L.; Journet, C.;

Bernier, P.; Bryne, H. J.; Carroll, D.; Ajayan, P. M.; Lefrant, S.; Blau, W. *Synth. Met.* **1999**, *103*, 2559.

37. Hirsch, A. *Angew. Chem., Int. Ed.* **2002**, *41*, 1853-1859.
38. Fukushima, T.; Kosaka, A.; Ishimura, Y.; Yamamoto, T.; Takigawa, T.; Ishii, N.; Aida, T. *Science* **2003**, *300*, 2072-2074.
39. Coleman, J. N.; Dalton, A. B.; Curran, S.; Rubio, A.; Davey, A. P.; Drury, A.; McCarthy, B.; Lahr, B.; Ajayan, P. M.; Roth, S.; Barklie, R. C.; Blau, W. J. *Ad*V*. Mater.* **2000**, *12*, 213-216.
40. Vigolo, B.; Penicaud, A.; Coulon, C.; Sauder, C.; Pailler, R.; Journet, C.; Bernier, P.; Poulin, P. *Science* **2000**, *290*, 1331-1334.
41. Launois, P.; Marucci, A.; Vigolo, B.; Bernier, P.; Derre, A.; Poulin, P. *J. Nanosci. Nanotechnol.* **2001**, *1*, 125-128.
42. Poulin, P.; Vigolo, B.; Laonois, P. *Carbon* **2002**, *40*, 1741-1749.
43. O'Connell, M. J.; Boul, P. J.; Ericson, L. M.; Huffman, C. B.; Wang, Y.; Haroz, E.; Kuper, C.; Tour, J.; Ausman, K. D.; Smalley, R. E. *Chem. Phys. Lett.* **2001**, *342*, 265-271.
44. Dror, Y.; Salalha, W.; Khalfin, R. L.; Cohen, Y.; Yarin, A. L.; Zussman, E. *Langmuir* **2003**, *19*, 7012-7020.,
45. Bandyopadhyaya, R.; Nativ-Roth, E.; Regev, O.; Yerushalmi- Rozen, R. *Nano Lett.* **2001**, *1*, 1
46. Ko, F.; Khan, S.; Ali, A.; Gogotsi, Y.; Naguib, N.; Yang, G.; Li, C.; Shimoda, H.; Zhou, O.; Bronikowski, M. J.; Smalley, R. E. *AIAA* **2002**.

47. Ko, F.; Han, W. B.; Khan, S.; Rahaman, A.; Zhou, O. *ASC 16th Annu. Tech. Conf.* **2002**.

48. Schreuder-Gibson, H.; Senecal, K.; Sennett, M.; Huang, Z.; Wen, J. G.; Li, W.; Wang, D.; Yang, S.; Tu Y.; Ren, Z.; Sung, C. *Proc. Electrochem. Soc.* **2000**, 2000-2012.

49. Zhang, Y., Huang, Z.M., Xu, X., Lim, C.T., Ramakrishna, S., *Chem Mater*., 2004, 16, 3406

50. Bognitzki, M., Hou, H., Ishaque, M., Frese, T., Hellwig, M., Schwarte, C., Schaper, A., Wendorff, J.H., Greiner, W., *Adv. Mater.* 2000, 12, 9, 637

51. Xie, Y., Qiao, Z.P., Chen, M., Liu, X.M., Qian, Y.T., *Adv.Mater.* 1999, 11, 1512

52. M. M. Hohman, Y. M. Shin, G. C. Rutledge, and M. P. Brenner, *Phys. Fluids,* 2001, **13**, 2221

53. J. J. Feng, *Phys. Fluids* **2002**, 14, 3912

54. F. J. Higuera, *J. Fluid Mech.* **2006**, 558, 143

55. F. J. Higuera *Phys. Fluids,* **2007**, 19, 012102

56. Sun, Z., Zussman, E., Yarin, A., Wendorff, J.H., Greiner, A., *Adv Mater*., 2003, 15, 22, 1929

57. Ren, Z. F.; Huang, Z. P.; Xu, J. W.; Wang, J. K.; Bush, P.; Siegel, M. P.; Provencio, P. *Science* **1998**, *282*, 1105-1107.

Chapter 7

Conclusion and future work

The main objectives of our research were to understand the fundamentals of electrospinning and study effect of various process parameters associated with electrospinning such as applied electric field, feed rate, distance between tip and grounded electrode; and solution parameters such as molecular weight of polymer, viscosity, surface tension, and concentration of polymer solution. Based on these understandings, an additional aim was to fabricate novel electrospun mats for applications including tissue engineering scaffolds.

Nylon-6 was selected as the first step to figure out intricacies of electrospinning. Through a comprehensive series of experiments using different Mw (30,000, 50,000, 63,000 gm/mol) and concentration (10, 15 wt %) of nylon-6, we were able to identify factors which affect the morphology of nanofibers. As Mw increased, chain entanglement density also increased which is a favorable factor in production of nanofibers. However with an increase in Mw, viscosity and surface tension also increases which impedes production of nanofibers. These contradicting effects of variation in Mw, makes electrospinning process very specific and exclusive for a certain polymer having a particular Mw.

As a consequence of increased chain entanglement density at high Mw, nanofibers were produced at relatively low concentration of high Mw as compared to low Mw nylon-6. Change in surface tension was insignificant as compared to viscosity with a variation in

Mw and concentration of polymer. A detailed investigation into the role played by process parameters was also conducted. It was found that with an increase in voltage uniform nanofibers with larger diameters were formed. Similarly, diameter also increased with an increase in feed rate of polymer solution. However, with increasing tip to collector distance, a diminishing trend in diameter of nanofibers was observed.

Mechanical testing showed that with an increase in Mw, tenacity as well as modulus of nanofibrous mats increased. This indicates that both fiber strength and the strength at fiber-fiber junctions increased. Future studies focusing on molecular interactions at fiber-fiber weld points are required to obtain a better understanding of the entanglement mechanism at increased molecular weight.

Observations made in the study of nylon-6 were utilized to gain an insight and acquire sufficient knowledge about the electrospinning process, which would further be utilized for developing a model to be used to produce coaxial nanofibers.

Chitosan nanofibers were obtained using coaxial syringe system. Chitosan is difficult to electrospin owing to its inherent solution properties such as hydrogen bonding, high viscosity and tendency to form gels. For this purpose PEO was used as sheath to support formation of chitosan nanofibers as core inside. PEO being soluble in water, was subsequently dissolved by treatment of the nanofibrous mats with de-ionized water, leaving chitosan nanofibers. This was confirmed by Fourier Transform Infrared Spectroscopy (FTIR). SEM investigation showed that morphology of coaxial nanofibers

was same as single layer nanofibers. TEM study revealed the core-sheath structure of nanofibers, verifying the result obtained from FTIR. Future work would include production of such nanofibrous mats to be employed for tissue engineering and wound healing scaffolds, taking into consideration the anti-bacterial properties of chitosan.

Core-sheath nanofibers involving only one polymer (PEO) were produced by using the same set-up employed to produce chitosan (core)-PEO (sheath) nanofibers. The main objective of this research was to realize high conductivity in nanofibers. With this intention sheath layer was doped with multi-walled carbon nanotubes (MWNTs) and core material was pure polymer. Percolation threshold was observed at 0.25 wt % in case of coaxial nanofibers as compared to 0.5 wt % MWNT concentration in single layer nanofibers. TEM images verified core-sheath structure. At concentration higher than 0.25 wt %, nanotube aggregation was observed, which acts as stress concentration points resulting in reduction of mechanical properties.

Such an increase in conductance at lower concentrations of MWNTs is advantageous since MWNTs have not been produced at commercial level yet and are, therefore, expensive. Additionally, reduced nanotube concentrations will also be advantageous for reducing the risk of toxicity in biological applications. Future work would include utilization of such novel nanofibers in cell-culture to assess the potential of MWNTs in mimicking natural milieu as found in human body by simulating electrical pulses through the electrospun nanofibrous mats. With this we would also be able to address how these

core-sheath structures will affect attachment, growth, proliferation and differentiation of cells in tissue engineering strategies.